

Dissertation zur Erlangung des Doktorgrades
der Fakultät für Chemie und Pharmazie
der Ludwig-Maximilians-Universität München



**Biochemical and Functional Analysis of a Genetic Mouse Model
with Altered HCN Channel Expression**

Zhuolu Niu

aus

Yaan, Sichuan, P.R.China

2015

Erklärung

Diese Dissertation wurde im Sinne von § 7 der Promotionsordnung vom 28. November 2011 von Herrn Prof. Dr. Martin Biel betreut.

Eidesstattliche Versicherung

Diese Dissertation wurde eigenständig und ohne unerlaubte Hilfe erarbeitet.

München, den 24. April 2015

Zhuolu Niu

Dissertation eingereicht am	20.03.2015
1. Gutachter	Prof. Dr. M. Biel
2. Gutachter	Prof. Dr. C. Wahl-Schott
Mündliche Prüfung am	21.04.2015

Table of contents

1.	Introduction.....	1
1.1	Aim of the study	8
2.	Materials and Methods	9
2.1	Chemicals, solutions and buffers.....	9
2.2	Experimental animals	9
2.3	Biochemical experiments	9
2.3.1	Tissue preparation.....	9
2.3.2	Genotyping	9
2.3.3	RNA analyses	10
2.3.3.1	Isolation and quantification of RNA	10
2.3.3.2	Reverse transcription	11
2.3.3.3	Northern blot analysis	11
2.3.3.4	<i>In situ</i> hybridization	13
2.3.3.5	Quantitative real-time PCR.....	15
2.3.4	Protein analyses	16
2.3.4.1	Isolation and quantification of proteins	16
2.3.4.2	Deglycosylation assay.....	16
2.3.4.3	Western blot analysis	17
2.3.4.4	Immunohistochemistry	17
2.3.5	Histological analysis.....	17
2.4	Behavioral tests	18
2.4.1	Animal housing	18
2.4.2	Assessment of body growth and longevity study.....	18
2.4.3	Footprint analysis	18

2.4.4	Open field test	19
2.4.5	Visual discrimination task.....	19
2.5	EEG measurements	20
2.6	Optical coherence tomography (OCT).....	22
2.7	Statistical analysis.....	22
3.	Results	23
3.1	Generating HCN2-1 switch mice.....	23
3.2	Biochemical analyses of HCN2-1 switch mice	23
3.2.1	Absence of HCN2 mRNA in HCN2 ^{sw/sw} mice.....	24
3.2.2	Expression of FLAG-HCN1 mRNA in HCN2 ^{sw/sw} mice	26
3.2.3	Unaltered HCN3 and HCN4 expression levels in HCN2 ^{sw/sw} mice	28
3.2.4	Regional expression pattern of FLAG-HCN1 mRNA in HCN2 ^{sw/sw} mice	28
3.2.5	Expression of FLAG-HCN1 proteins in HCN2 ^{sw/sw} mice	31
3.2.6	Glycosylation of FLAG-HCN1 proteins	33
3.2.7	Immunohistochemistry analysis of FLAG-HCN1 distribution in HCN2 ^{sw/sw} mice ...	34
3.3	Normal brain morphology in HCN2 ^{sw/sw} mice	37
3.4	Behavioral tests of HCN2-1 switch mice.....	38
3.4.1	Reduced body size and shortened lifespan in HCN2 ^{sw/sw} mice.....	38
3.4.2	Ataxic gait in HCN2 ^{sw/sw} mice	40
3.4.3	Motor deficit in HCN2 ^{sw/sw} mice	43
3.4.4	Impaired visual discrimination capacity in HCN2 ^{sw/sw} mice.....	44
3.5	Spike-and-wave discharges in HCN2 ^{sw/sw} mice	47
4.	Discussion	49
5.	Summary.....	55
6.	Literatures	57
7.	Appendix.....	62

7.1 Abbreviations.....	62
7.2 Primers.....	66
7.2.1 HCN2-1 switch genotyping	66
7.2.2 HCN1 genotyping.....	66
7.2.3 Primers for northern blot	66
7.2.4 Primers for <i>in situ</i> hybridization	67
7.2.5 Primers for qPCR.....	67
7.3 Primary antibodies.....	67
7.4 Secondary antibodies	68
7.5 Alignment of the primary sequences of mHCN1 and mHCN2.....	68
7.6 Nucleotide sequence of the HCN2-1 switch allele	69
7.7 Acknowledgement.....	71

1. Introduction

Since the hyperpolarization-activated current (I_h) was first discovered in spontaneously active cells (neurons and sinoatrial node cells) (DiFrancesco, 1981; Halliwell and Adams, 1982), the biological functions of I_h in the regulation of neuronal excitability and cardiac pacemaker mechanisms have been intensively studied. Activated by hyperpolarization, I_h depolarizes the membrane potential toward the threshold for firing an action potential. Cyclic nucleotides (e.g. cAMP, cGMP and cCMP) regulate I_h by shifting its activation curve to a more depolarized potential (DiFrancesco and Tortora, 1991; Zong et al., 2012). In neurons, I_h plays a key role in the generation and regulation of neuronal rhythmicity, e.g. in thalamocortical relay (TC) neurons, the activation of I_h slowly depolarizes the membrane potential toward the threshold for a burst of action potentials (Figure 1A) (McCormick and Pape, 1990). Besides, I_h is also involved in determination of resting membrane potential (Ludwig et al., 2003; Nolan et al., 2007; Huang et al., 2009), dendritic integration (Shah et al., 2010; Pavlov et al., 2011; Harnett et al., 2015) and synaptic transmission (He et al., 2014; Huang and Trussell, 2014). In heart, I_f (funny current) contributes to the initiation and regulation of heart beats by generating spontaneous diastolic depolarization (Figure 1B) (Mangoni and Nargeot, 2008).

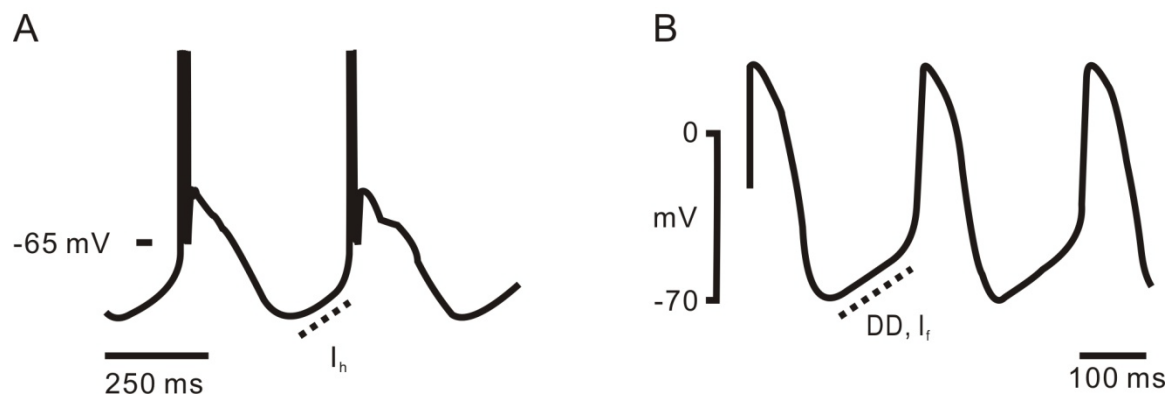


Figure 1: The role of I_h in the generation of pacemaker currents. (A) The tonic firing model of thalamocortical neurons. I_h is indicated by a dashed line. (B) Diastolic depolarization (DD) in sinoatrial node cells. I_f is indicated by a dashed line. Time scale is shown as a black bar. Adapted from the review of Biel et al. 2009.

The hyperpolarization-activated cyclic nucleotide-gated (HCN) channels underlying I_h belong to the superfamily of voltage-gated pore-loop cation channels. HCN channels are encoded by the *HCN1-4* genes in mammalian cells (Ludwig et al., 1998). Four subunits assemble to form a homomeric or heteromeric tetramer with a centrally located Na^+/K^+ -permeation pore (Figure 2, right). Each HCN subunit contains the typical structure of the voltage-gated potassium (Kv) channels, including cytoplasmic N- and C-termini, six transmembrane segments (S1-S6) and an ion-conducting pore loop between S5 and S6 segments (Figure 2, left). The positively charged voltage sensor (S4) carrying seven arginine and two lysine residues spaced at every third position is coupled to channel gating (Biel et al., 2009; Ryu and Yellen, 2012). The selectivity filter in the pore region contains a glycine-tyrosine-glycine (GYG) motif that forms the selectivity filter for potassium ions in the Kv channels (Macri et al., 2012). Although HCN channels show a higher selectivity for K^+ than for Na^+ , they still carry an inward Na^+ current under physiological conditions (Ludwig et al., 1998). The proximal C-terminus contains an 80-amino acid C-linker and a 120-amino acid cyclic nucleotide binding domain (CNBD). The CNBD is highly conserved in the superfamily of cyclic nucleotides-gated cation channels, consisting of three α -helices (A-C) and one eight-stranded antiparallel β -sheet ($\beta 1$ - $\beta 8$) between the A and B helices. Binding of cyclic nucleotides to the CNBD facilitates the activation of HCN channels. The C-linker with six α -helices (A'-F') contributes to the inter-subunit contact in the cAMP-dependent gating (Akimoto et al., 2014; Puljung et al., 2014; Kesters et al., 2015).

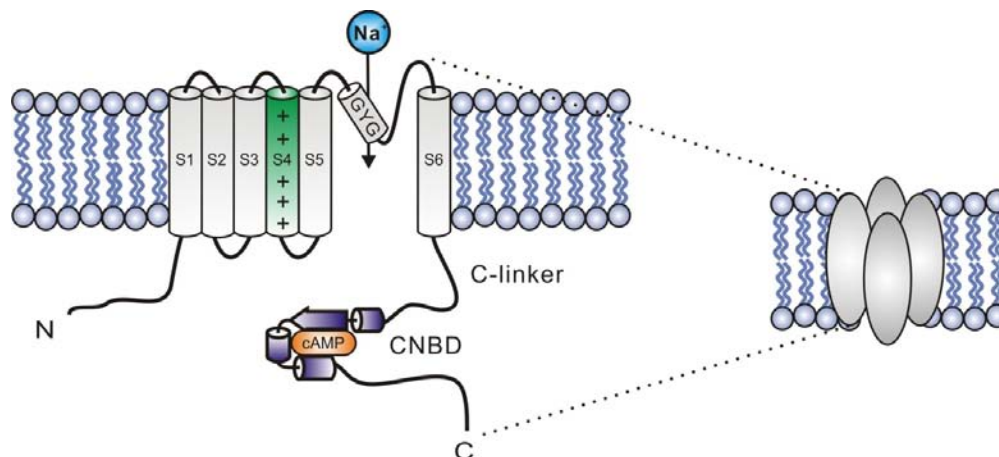


Figure 2: The structure of HCN channel. An HCN channel is a tetramer (right). Each monomer (left) contains six transmembrane segments (S1-S6), among which S4 is the voltage sensor and the S5 and S6 form an ion-conducting pore. The selectivity filter contains the GYG motif that is specific for Kv channels. The cytosolic C-linker connects the CNBD and the distal C-terminus to the transmembrane channel core.

In the heterologous expression system, the homomeric HCN1 and HCN2 channels generate distinct I_h with distinguishable steady-state voltage-dependence and cAMP sensitivity. Generally, HCN1 activates at more depolarizing potential and has a faster activation kinetic than HCN2. However, HCN2 can be strongly modulated by cAMP while HCN1 only responds weakly to cAMP binding (Table 1) (Wahl-Schott and Biel, 2009). Lolicato et al. (2011) proposed that HCN1 is insensitive to cAMP due to its partially occupied CNBD domain at the basal cAMP concentration, where the tetrameric assembly of HCN1 subunits already begins. By contrast, the CNBDs of HCN2 require a saturated cAMP concentration to start the heteromerization.

Table 1. Biophysical properties of homomeric HCN1 and HCN2 channels

	HCN1	HCN2
$V_{1/2}$	-70 mV	-95 mV
τ	25-300 ms	hundreds of ms
$\Delta V_{1/2}$ (with cAMP)	about + 5 mV	+12 to +17 mV
fold-change of τ (with cAMP)	1.5-fold	3.5-fold

Data are adapted from the review of Wahl-Schott and Biel (2009).

All four HCN channels are expressed in the central nervous system (CNS). HCN1 is abundantly expressed in the neocortex, hippocampus olfactory bulb and cerebellum. HCN2 is broadly expressed throughout the CNS, with the highest level in the thalamus and brain stem nuclei. HCN3 is only distributed in the olfactory bulb and in some hypothalamic nuclei at moderate to high level. HCN4 is strongly expressed in the thalamus and olfactory bulb (Moosmang et al., 1999; Santoro et al., 2000; Notomi and Shigemoto, 2004). *In vivo*, the native I_h properties are determined by three factors: 1) heterogeneity of HCN subunits (Santoro et al., 2000). HCN subunits have been found to coassemble to form homo- and heteromers in the mouse brain (Chen et al., 2001; Much et al., 2003). 2) posttranscriptional modifications, e.g. glycosylation (Much et al., 2003; Wilkars et al., 2014; Li et al., 2015). 3) regulation by auxiliary subunits, such as TRIP8b, Filamin A and KCTD3 (Brager et al., 2013; Cao-Ehlker et al., 2013; He et al., 2014). The diversity of I_h in neurons is in line with its physiological functions in single neurons or neuronal networks.

HCN1 and HCN2 channels have different cellular distribution patterns that contribute to distinct functions of I_h in brain. For example, in the hippocampal CA1 and neocortical layer 5 pyramidal neurons, HCN1 is distributed with an increasing density with the distance from soma to distal apical dendrites while HCN2 is mainly expressed in the soma (Lorincz et al., 2002; Atkinson and Williams, 2009; Bittner et al., 2012; Harnett et al., 2015). The somatodendritic gradient of HCN1 is consistent with the distal enrichment of I_h . Activation of I_h reduces the membrane resistance and the neuronal time constant. Therefore, the distal EPSPs rise and decay more rapidly than the proximal EPSPs. This ensures an equal temporal summation of all inputs when they reach the soma. Comparably, the distal dendritic I_h enhances the attenuation of dendro-somatic IPSPs, leading to the inhibition of dendritic spike generation and the axonal action potential firing (Williams and Stuart, 2003; Pavlov et al., 2011). In the thalamus, HCN2 predominates while HCN1 is expressed at a low level. HCN2 is uniformly distributed in the thalamocortical relay (TC) neurons and abundantly in the distal dendrites of the thalamic reticular neurons (RTN) (Abbas et al., 2006). Because HCN2 is the dominant isoform, thalamic I_h activates slowly and can be effectively modulated by cAMP. The TC, RTN and corticothalamic (CT) neurons together build up the thalamocortical circuit, which is crucial for the generation and regulation of the thalamic rhythms (Figure 3A). The TC neurons generate action potentials in two distinct modes: burst firing and tonic firing. Under the physiological conditions, the former occurs in the non-rapid eye movement (NREM) sleep while the later in wakefulness and the REM sleep. During the burst firing, membrane hyperpolarization activates I_h followed by the activation of a low-threshold calcium current (I_T) beyond -65 mV. A series of Ca^{2+} spikes evoked by the activation of I_T subsequently cause a burst of Na^+/K^+ -dependent action potentials. Depolarization deactivates I_h and inactivates I_T resulting in repolarization. Then hyperpolarization deactivates I_T and activates I_h . In this way, the circle repeats. The transition between burst and tonic firing is regulated by several excitatory neurotransmitters (NTs), such as noradrenaline (NA), serotonin (5-HT), acetylcholine (ACh) and histamine (HA) derived from the ascending brainstem system. These NTs elevate the intracellular cAMP level and enhance the I_h activity. The elevated membrane potential suppresses the I_T -evoked Ca^{2+} spikes, thus terminates the burst firing mode (Figure 3B) (McCormick and Bal, 1997). The high distal dendritic density of I_T and I_h is important for the generation of burst firing in RTN neurons (Destexhe et al., 1996; Abbas et al., 2006), which initiate synchronized oscillations in the thalamocortical network to cause spindle wave activity at the early stage of NREM sleep.

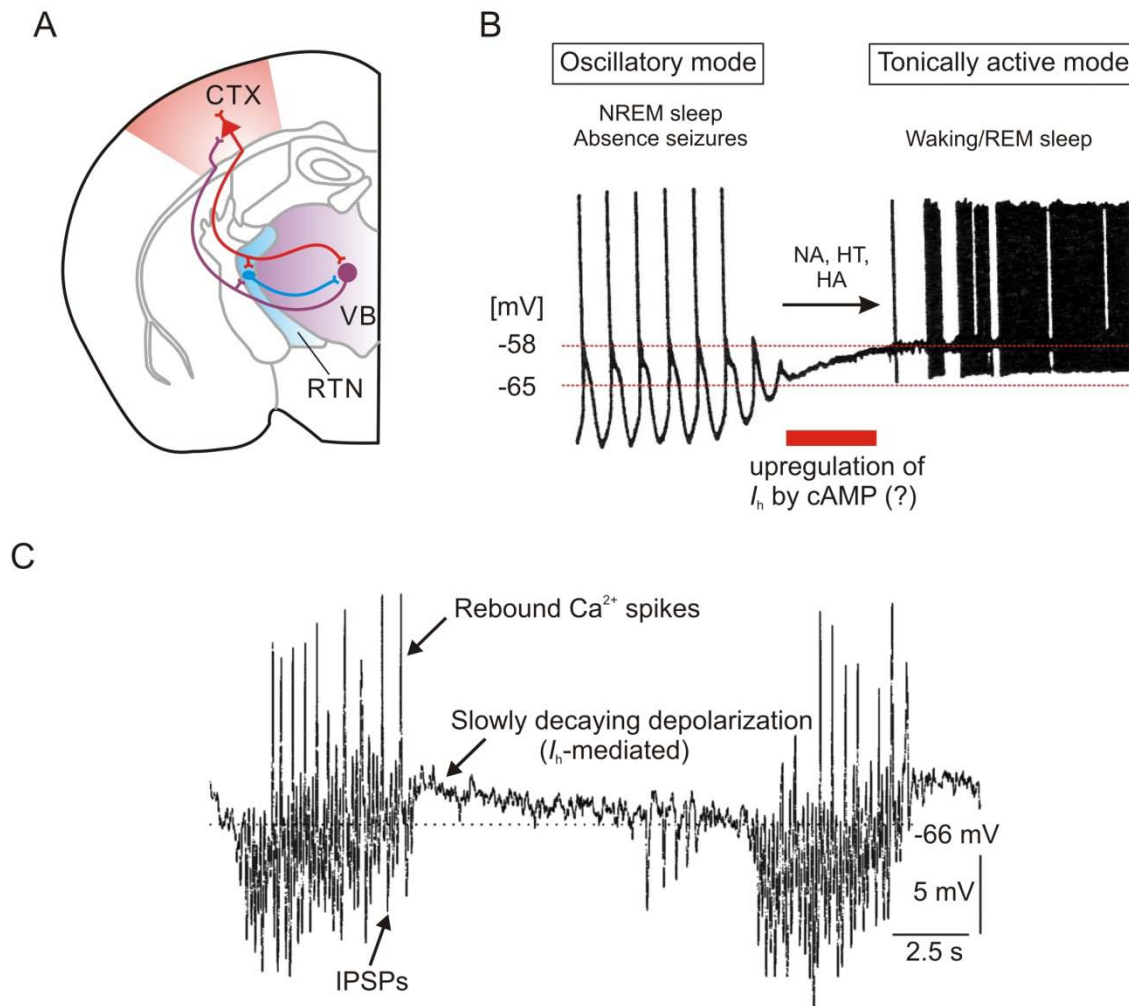


Figure 3: Physiological roles of I_h in the thalamocortical circuit. (A) Overview of the thalamocortical circuit in a mouse coronal section. CTX: somatosensory cortex, VB: ventral basal complex of thalamus, RTN: reticular thalamic nucleus. \blacktriangle : corticothalamic neuron, \bullet : thalamocortical relay neuron, \circ : thalamic reticular neuron, red and purple lines : excitatory glutamatergic pathways, blue line: inhibitory GABAergic pathway. (B) Firing modes of the thalamocortical neurons. (C) Generation of spindle activity. (Modified from McComick and Bal, 1997)

The inhibitory postsynaptic potentials (IPSPs) generated by the burst firing of GABAergic RTN neurons hyperpolarize the TC neurons followed by the activation of I_T and I_h . The resulting depolarization generates a rebound Ca^{2+} spike and a burst of action potentials, which in turn stimulate both RTN and CT neurons and give rise to spindle waves (frequency 6-14 Hz, duration 1-4 s) in the widespread cortical areas. The silence period (duration 5-20 s) between two spindles is a consequence of the persistent activation of I_h by cAMP binding. The elevated cAMP level in TC neurons result from the activation of the Ca^{2+} -sensitive adenylyl cyclases by the

rebound Ca^{2+} spike. The enhanced I_h in turn suppresses the burst of action potential until I_h slowly decays (Figure 3C) (McCormick and Bal, 1997; Biel et al., 2009).

Absence epilepsy is a kind of generalized seizures with a spontaneous loss of consciousness. During absence seizures, synchronized oscillations at 3-4 Hz are generated in the thalamocortical circuit and characterized by the bilateral spike-and-wave discharges (SWDs) in EEG. The mouse model with a complete ablation of HCN2 subunits provides a compelling evidence for the linkage between the I_h dysfunction and absence epilepsy (Ludwig et al., 2003). The loss of functional HCN2 channels in TC neurons leads to a reduction in I_h by about 80% and a hyperpolarizing shift of the resting membrane potential by about +12 mV. These alterations remove the inactivation of T-type calcium channels and promote the burst firing when excitatory stimulus is present. The increased oscillatory activity in TC neurons in turn increases the seizure susceptibility. Another mouse model displaying absence seizure is the apathetic (ap/ap) mice, in which a spontaneous insertion of a TTCA sequence into the exon 6 of the native *HCN2* gene completely disrupts the expression of HCN2 protein (Chung et al., 2009). The ap/ap mice show frequent SWDs in cortical EEG. Furthermore, a recent study on another absence epileptic mouse model, the *tottering* mice, has been revealed that the generation of cortical SWDs is related to the increased membrane excitability of subthalamic neurons (STN) due to a reduced I_h activity (Kase et al., 2012).

The mouse models mentioned above demonstrate an essential role of HCN2 channels in the epileptogenesis. However, the contribution of HCN1 to the epileptogenesis is unclear. The global or forebrain-restricted knockout mice do not exhibit epileptic seizures. The HCN1-null mice show profound motor learning and memory deficits (Nolan et al., 2003) and the HCN1 forebrain-restricted knockout mice exhibited improved spatial learning and memory (Nolan et al., 2004). Huang et al. (2009) demonstrated that the genetic deletion of HCN1 channels ablates the dendritic I_h in entorhinal cortex (EC) layer III neurons resulting in a more hyperpolarized RMP and an enhanced integration of EPSPs. The hyperexcitability of cortical pyramidal neurons promotes the seizure susceptibility in temporal lobe epilepsy (Poolos, 2010). Supportively, studies in two independent epileptic rat models, Wistar Albino Glaxo rats bred in Rijswijk (WAG/Rij) and Generalized Absence Epilepsy Rat from Strasburg (GAERS), have been revealed that HCN1 channels are involved in the genesis of epileptic seizures. In these studies, HCN1 is up-regulated in the thalamus, leading to a less responsiveness to cAMP modulation and thus

promotion of burst firing (Budde et al., 2005; Kuisle et al., 2006; Kanyshkova et al., 2012). In addition, HCN1 is down-regulated in the somatosensory cortex, leading to a reduced I_h activity and augmented membrane excitability (Strauss et al., 2004; Polack et al., 2007; Polack et al., 2009; van Luijtelaaar et al., 2011).

To determine the impacts of cAMP-dependent HCN channel modulation and voltage-dependent HCN channel activation on the regulation of the rhythmic activity in TC neurons and the oscillatory activity in the thalamocortical circuit, a novel HCN2 replacement mouse model, i.e. HCN2-1 switch mice, has been developed (unpublished data from the laboratory of Prof. Dr. Martin Biel, Ludwig-Maximilians Universität München) (Figure 4, Appendix 7.6). In HCN2-1 switch mice, a coding sequence of mHCN1 tagged with a triple FLAG at the N-terminus replaces the exon 1 of the *HCN2* gene, resulting in an expression of FLAG-HCN1 instead of HCN2 in the HCN2 locus.

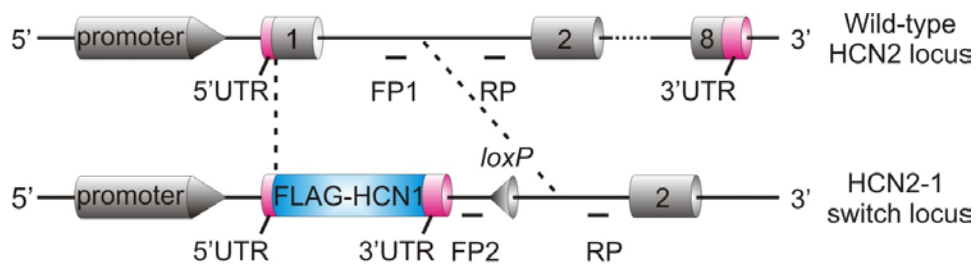


Figure 4: Generation of HCN2-1 switch mice. Exon 1 of the native *HCN2* gene (upper) is replaced by a FLAG-HCN1, generating a novel HCN2-1 switch mouse strain (bottom). The replacement area is indicated by two dashed lines. The transcription of FLAG-HCN1 is under the control of native HCN2 promoter. Primers for genotyping (FP1, FP2 and RP) are indicated by short lines.

1.1 Aim of the study

HCN channels function as pacemakers in the regulation of neuronal network activities in the CNS. HCN1 and HCN2 differ from each other in their biophysical properties. HCN1 shows a fast activation kinetic whereas HCN2 displays a slower activation. Furthermore, HCN2 is highly regulated by cAMP while HCN1 is only weakly (if at all) affected. The relevance of these differences in the HCN1 and HCN2 channel properties to the neuronal function remains unknown.

To address this question *in vivo*, a genetic HCN2-1 switch mouse model has been generated, in which the cDNA of a FLAG-HCN1 channel was introduced into exon 1 of the *HCN2* gene. As a result, these mice express the FLAG-HCN1 channels under the control of the HCN2 promoter. Moreover, they no longer express the HCN2 channels. Biochemical analyses should be performed to verify the expression of FLAG-HCN1 at mRNA and protein levels using biochemistry and molecular biology techniques, such as northern blot, *in situ* hybridization, western blot and immunohistochemistry. The expression level of HCN3 and HCN4 in HCN2-1 switch mice should be determined to exclude the impact from the alterations in HCN1 and HCN2. As reported, loss of HCN2 resulted in evident changes in body size and behavioral phenotypes, it is important to investigate whether the newly generated FLAG-HCN1 in the HCN2 locus could rescue or attenuate phenotypes caused by deletion of HCN2. For this purpose, HCN2-1 switch mice should be characterized and compared with WT and HCN2-null mice in a set of behavioral tests, such as body growth assessment, foot print analysis, open field test and visual discrimination task. Finally, EEG measurements should be performed to analyze the occurrence of SWDs in HCN2-1 switch mice.

2. Materials and Methods

2.1 Chemicals, solutions and buffers

All chemicals were purchased from Merck, Roth and Sigma-Aldrich if not specially mentioned. The quality of chemicals was “pro analysi” or “for molecular biological use”. All solutions and buffers were prepared with ultrapure deionized water (Milli-Q® gradient water purification system, Millipore).

2.2 Experimental animals

The mouse strain, HCN2-1 switch, was generated and bred in our own laboratory. The chimeric mice were backcrossed for three to four generations into the C57B/6J strain. Maintenance and experimental processes of HCN2-1 switch mice were permitted by the “Regierung von Oberbayern” with the official sign code 55.2-1-54-2532-172-11.

The HCN1^{-/-}/HCN2^{sw/sw} mice were obtained by a cross of HCN1^{+/-}/HCN2^{+sw} mice, which were developed by crossing HCN1^{-/-} with HCN2^{+sw} first.

2.3 Biochemical experiments

2.3.1 Tissue preparation

Adult mice aged at 8-10 weeks in either sex were used for the biochemical experiments. Tissue samples were taken from the mice sacrificed by cervical dislocation. Fresh mouse brains were either immediately used for experiments or frozen in isobutane at -25°C followed by section preparation on the Leica CM3050 S cryostat. Brain regions were dissected from a single brain and frozen in liquid nitrogen for use.

2.3.2 Genotyping

Genomic DNA was extracted from mouse ear biopsies using proteinase K (50 U/ml, Roche) in 1x buffer at 55°C for 1 hour. Genotyping was performed with a multiplex PCR using three specific primers (Appendix 7.2.1 and 7.2.2).

10x proteinase K buffer		PCR Reaction mixture (25 μ l)	
100 mM	Tris-HCl, pH 8.0	1x	PCR buffer with MgCl ₂
5 mM	EDTA	1.6 mM	dNTPs
0.2%	SDS	5 pmol/ μ l	primers for each
200 mM	NaCl	0.25 μ l	<i>Taq</i> polymerase
	adjust to pH 8.5	4 μ l	DNA sample

PCR program	HCN2-1 switch			HCN1		
Initial denaturation	95°C	3 min		95°C	3 min	
Denaturation	95°C	1 min				
Annealing	72°C	30 sec	5 cycles	-		
Elongation	72°C	30 sec				
Denaturation	95°C	1 min		95°C	1 min	
Annealing	67°C	30 sec	25 cycles	67°C	30 sec	30 cycles
Elongation	72°C	30 sec		72°C	30 sec	
Final elongation	72°C	5 min		72°C	5 min	

2.3.3 RNA analyses

To avoid RNase contamination, the Milli-Q® water was further treated with DEPC (0.1% v/v, AppliChem) over night followed by autoclaving for twice. All glassware and metalware were baked at 200°C over night. Filter pipette tips and tubes (VWR) were free of DNA and nucleases (RNase/DNase). The operation surfaces were wiped clean with RNASE AWAY® (Thermo Scientific).

2.3.3.1 Isolation and quantification of RNA

Total RNA was extracted from the mouse brain using the peqGOLD TriFase™ reagent (Peqlab) following the manufacture's instruction. The isolation of polyA⁺ mRNA was conducted by hybridizing the total RNA to an oligo(dT)-cellulose column built by applying 0.1 g of oligo(dT)-cellulose per 0.5 mg of total RNA into a Poly-Prep® chromatography

column (Biorad). After equilibration with binding buffer, 450 µg of total RNA was loaded to the oligo(dT)-cellulose column and the flow-through was reloaded twice. To remove the non-mRNA components from the oligo(dT)-cellulose column, it was washed with ten column volumes of binding buffer until the RNA concentration in the flow-through was nearly zero. Next, two column volumes of elution buffer were applied to the oligo(dT)-cellulose column and the eluted mRNA was precipitation of mRNA using sodium acetate/2-propanol. The concentration of total RNA or mRNA in the preparations was determined photometrically using the RNA assay program (A_{260}) by a BioPhotometer (Eppendorf).

Binding buffer	Elution buffer
0.5 M NaCl	10 mM Tris-HCl, pH 7.5
10 mM Tris-HCl, pH 7.5	1 mM EDTA, pH8.0
1 mM EDTA, pH 8.0	0.05% SDS

2.3.3.2 Reverse transcription

First-strand cDNA was primed with oligo(dT) from 0.5 µg of total RNA extracted from the mouse brain and synthesize cDNA with the RevertAid® First cDNA synthesis kit (Thermo scientific) according to the manufacture's instruction.

2.3.3.3 Northern blot analysis

Two micrograms (2µg) of mRNA sample were denatured with 2x RNA loading dye at 99°C for 10 min. The denatured mRNA was then separated by electrophoresis on a formaldehyde agarose gel in 1x MOPS buffer. After transferring onto a nylon membrane (Genescreen plus, Perkin Elmer), the blot was irradiated by UV-light with an energy intensity of 120 mJ/cm² (CI-1000 Ultraviolet Crosslinker, UVP).

DNA template for the probe labeling was amplified from the brain cDNA of a WT mouse using specific primers (Appendix 7.2.3) followed by a purification with QIAquick Gel Extraction Kit (Qiagen). The purified DNA template was then labeled with ³²P-desoxycytidintriphosphat

(Perkin Elmer, 37 MBq) by Random Prime Labeling Kit (Roche) according to the manufacture's instruction, with minor modifications. The ^{32}P labeled probe was purified with Nick column (GE-Healthcare). 2 μl of purified probe was supplied to the LS 6500 Multi Purpose Scintillation Counter (Beckman) for radioactivity measurement.

2x RNA loading-dye		10x MOPS	
50%	Deionized formamide	200 mM	MOPS
17.5%	Formaldehyde	50 mM	Sodium acetate
10%	10x MOPS	10 mM	EDTA, pH 8.0
5%	Glycerol		Adjust pH to 7.0 with
0.25%	0.5 M EDTA, pH 8.0		NaOH, stored at 4°C in
0.5%	Ethidium bromid		dark
0.025%	Bromphenol blue		

^{32}P-dCTP Labeling reaction pro probe		
200 ng	DNA template	
ad 14 μl	H ₂ O	99°C, 10 min
6 μl	dNTPs (-dCTP)	
4 μl	10x reaction mix	
14 μl	$\alpha^{32}\text{P}$ -dCTP	
2 μl	Klenow enzyme	37°C, 1.5 h

After pre-hybridization, the blot was incubated in the hybridization buffer containing ^{32}P labeled probe (3.3×10^5 cpm/cm²) at 42°C over night with rotation. After several intensive washes with graded SSC buffers containing 0.1% SDS, the radioactivity of the blot was lower than 100 IPS. The target mRNA was visualized by autoradiography on a phosphoimager plate (BAS-MP 2040S, Fujifilm).

Pre-hybridization buffer		Hybridization buffer		
1x	PE buffer	1x	PE buffer	
5x	SSC	5x	SSC	
50%	Deion. formamide	50%	Deion. formamide	
0.15 mg/ml	ssDNA	0.15 mg/ml	ssDNA	
ad. 10 ml	H ₂ O	5x 10 ⁶ cpm/ml	³² P - probe	

5x PE buffer		20x SSC		
0.5%	Tetrasodium pyrophosphate decahydrate	0.3M	Sodium citrate dihydrate	
1%	PVP 40,000		3M NaCl	
1%	Ficoll 400,000		adjust pH to 7.0	
1%	SDS			
250 mM	Tris-HCl, pH 7.5			
25 mM	EDTA, pH 8.0			
1%	BSA (Fraction V) steril filtrate			

2.3.3.4 *In situ* hybridization

To obtain RNA templates for riboprobe synthesis, *in vitro* transcription was performed. A fragment of target mRNA was amplified from the mouse brain cDNA with specific primers (Appendix 7.2.4). Then the target mRNA fragment was cloned into a pBluescript SK⁻ (Stratagene) plasmid using Kpn I and Sac I restriction sites. After linearization of the pBSSK⁻ plasmid with Kpn I or Sac I respectively, the sense strand was transcribed *in vitro* under the control of T7 promoter and the antisense strand under the control of T3 promoter using ³⁵S-UTP (1mCi, Perkin Elmer), SP6/T7 transcription kit (Roche) and T3 RNA polymerase (Roche) according to the manufacture's instruction. The riboprobes were extracted from the reaction mixture using phenol/chloroform and purified through a Nick column. The radioactivity was measured with 3 ml of scintillation fluid containing 2 µl of riboprobe on the LS 6500 multipurpose scintillation counter (Beckman).

***In vitro* transcription**

1.5 µg	pBSSK ⁻ (dig. with Kpn I or Sac I)	
	dried and dissolved in 3 µl H ₂ O	
1.5 µl	10x transcription buffer	
0.75 µl	RNase inhibitor	
0.25 µl	0.75 M DTT	
0.5 µl	ATP/CTP/GTP each	
7 µl	³⁵ S – UTP	
1 µl	T3 or T7 RNA polymerase	37°C, 1 h
0.5 µl	DNase I	37°C, 10 min

Sagittal sections (12 µm) of the mouse brain were fixed in 4% PFA (pH 7.4) for 30 min and digested with proteinase K for 15 min. The sections were then incubated in TEA solution with 0.25% acetic anhydride followed by a gradient ethanol treatment. The dehydrated sections were pre-hybridized in 1x hybridization buffer at 42°C for 3 h. The ³⁵S labeled riboprobe was denatured at 65°C for 10 min followed by adding DTT to get a final concentration of 75 mM. After pre-hybridization, the sections were incubated with the denatured riboprobe at 55°C overnight. The hybridized sections were exposed to RNase A solution (20 µg/ml) for 30 min to disrupt non-hybridized RNA. After several intensive washes in decreasingly gradient SSC buffers, the sections were dehydrated with 70-100% ethanol containing ammonium acetate. The target mRNA was visualized on a Biomax MR film (Cat. 8736936, Kodak) by autoradiography.

Protease K solution

9 µg/ml	Proteinase K (20mg/ml)
1x	Proteinase buffer

5x proteinase buffer

0.1 M	Tris-HCl, pH 8.0
5 mM	EDTA, pH 8.0

5x RNase buffer		1.25x hybridization buffer	
0.5 M	NaCl	10 mM	Tris-HCl, pH 8.0
10 mM	Tris-HCl, pH 8.0	0.3 M	NaCl
1 mM	EDTA, pH 8.0	1 mM	EDTA, pH 8.0
		1x	Denhardt
		10%	Dextran
		50%	Deion. formamide

2.3.3.5 Quantitative real-time PCR

Quantitative PCR was performed using the KAPA SYBR® FAST qPCR Kit Master Mix Universal (2x) (Peqlab) and with the exon spanning primers (see Appendix 7.2.5) on the Light Cycler® 480 (Roche) according to the manufactures' instruction. All applications of different cDNA input were performed in triplets (WT1-3, SW 1-3 etc.). The mean threshold cycle (C_t) from duplicated measurements of each cDNA sample was calculated for further analyses. The annealing temperature for all PCRs was set to 65°C to ensure a specific binding to the target gene. The amplification efficiency was calculated for each pair of primers using a standard curve from five sample dilutions (1:3, 1:5, 1:25, 1:125 and 1:625). Relative quantification was done using the comparative $\Delta\Delta C_t$ method. Delta-aminolevulinatase synthase (ALAS) was used as reference gene.

Step	Temp.	Duration	Cycles	Analysis mode
Initial denaturation	94°C	3 min	1	None
Denaturation	94°C	30 sec		None
Annealing	65°C	10 sec	45	None
Elongation	72°C	5 sec		Quantification
Melting	95°C	∞		Melting curve

2.3.4 Protein analyses

2.3.4.1 Isolation and quantification of proteins

For the membrane protein preparation, mouse brain was homogenized in 2 ml of 1x membrane lysis buffer containing proteinase inhibitor cocktail mix (EDTA-free, roche) using the Potter S homogenizer (900 rpm, 10 strokes). The lysate was centrifuged at 5000 g for 10 min at 4°C and the supernatant was further centrifuged at 30,000 rpm for 45 min at 4°C in a 45 Ti tube. After centrifugation, the supernatant was discarded and the pellet was resuspended in 100 µl of 1x membrane lysis buffer.

For the whole cell protein preparation, mouse brain was homogenized in 500 µl of Tx lysis buffer containing proteinase inhibitor cocktail mix (EDTA-free, roche) using the Potter S homogenizer (900 rpm, 10 strokes). The lysate was rotated for 30 min at 4°C followed by centrifuging at 13,000 rpm for 15 min. The supernatant was further used for western blot analysis.

The concentration of protein preparations was determined with the absorbance at 280 nm on the NanoDrop 2000c spectrophotometer (Peqlab).

3x membrane lysis buffer	Tx lysis buffer
60 mM MOPS	50 mM Tris-HCl, pH 7.4
0.9 M D(+)-sucrose	1% Triton X-100
12 mM EDTA, pH 8.0	150 mM NaCl
Sterile filtrate, store at 4°C	1 mM EDTA, pH 8.0

2.3.4.2 Deglycosylation assay

Twenty micrograms (20µg) of membrane protein was treated with PNGase F (New England Biolabs) according to the manufacture's instruction.

2.3.4.3 Western blot analysis

Thirty micrograms (30 µg) of membrane proteins or 80 µg of whole cell proteins per lane were electrophoretically separated on an SDS-PAGE gel, and then transferred onto a PVDF membrane (Millipore, pore size 0.45 µm). After blocking in 5% milk powder solution for 30 min, the blot was incubated with an appropriate primary antibody (Appendix 7.3) at 4°C over night and with an appropriate secondary antibody (Appendix 7.4) at room temperature for 1 hour, consecutively. Then the blot was visualized using luminal reagents (Santa Cruz) by the ChemiDoc™ MP imaging system (Biorad).

2.3.4.4 Immunohistochemistry

Coronal or sagittal brain sections (12 µm thick) were fixed in 4% PFA for 5 min, followed by incubation in 10% normal goat serum (NGS) blocking solution containing 0.3% of Triton X-100 for 1 h at room temperature. After a further incubation with the primary antibody (Appendix 7.3) at 4°C over night, the sections were incubated with the secondary antibody (Appendix 7.4) for 1 h at room temperature. When required, a tyrosine signal amplification was performed using TSA plus cyanine 3 kit and the TSA plus fluorescein kit (PerkinElmer) following the manufacturer's instruction. The cell nuclei were counterstained using the Hoechst solution (5 µg/ml) for 5 min followed by embedding in the mounting medium (Life Technologies). Fluorescent images or confocal images were taken by the Axioplan2 fluorescence microscope or Leica TCS SP8 SMD Microscope.

2.3.5 Histological analysis

Coronal sections (25 µm thick) were dehydrated in 70% to 100% ethanol followed by staining with 0.5% cresyl-violet. The excessive stain was washed off with water, a series of water-ethanol mixtures and xylol, consecutively. The stained brain sections were embedded in Entellan® (Merck) under a cover slip and stored at room temperature. Images were taken with a stereo microscope (Stemi 2000, Zeiss).

2.4 Behavioral tests

2.4.1 Animal housing

In the mouse facility, mice were housed in the clean side under controlled conditions (temperature: 22°C, humidity: 60%, a 12h light-dark cycle with lights on at 7.00 a.m., food and water *ad libitum*). The food (R/M-H, 10 mm; Fa. Ssniff, Soest), water, cages (TypM2-L) with straw (Fa. Ssniff, Soest), cottage (ACRE011, Tecniplast), bedding and nesting materials (Fa. Ssniff, Soest) for the mice were all autoclaved before use. The floor area of a breeding cage was 1000 cm² and that of a housing cage was 700 cm². Four weeks after birth the pups were separated from their parents and raised in housing cages by sex. A maximum of five females or four males were allowed to live in one housing cage. Two females and one male were paired in one breeding cage. Two nestlets for one breeding pair and one cottage for single mouse were supplied.

The male HCN2^{sw/sw} mice and their WT littermates aged 8-10 weeks were housed individually in the housing cages in the testing room one week prior to the behavioral tests. The behavioral tests were performed between 12:00 AM and 6:00 PM.

2.4.2 Assessment of body growth and longevity study

Ten groups of HCN2^{sw/sw} and WT male littermates were individually housed in single cages after separation. Their body weights and survival rates were measured on a monthly basis for the duration of 20 months. Survival curves were plotted using the Kaplan-Meier method.

To measure body length of a mouse, it was anesthetized via inhalation of isoflurane in a sealed chamber after footprint analysis and the distance from the nose to the anus was measured.

2.4.3 Footprint analysis

Mice were trained to walk on a sheet of blank A4 paper along a runway (7 cm wide, 30 cm long). Their front and hind paws were painted with non-toxic paint in blue and green colors, respectively. The resulting footprint traces were analyzed by measuring the following morphometric parameters: front and hind base width (normalized to the body length), stride length and hind paw angle.

2.4.4 Open field test

An open grey box (50 cm x 50 cm x 50 cm; TSE systems) was used as the open-field arena. Mice were placed in the center of the arena and allowed to move freely for 5 min. The movement traces of the mouse were recorded by a video tracking system (VideoMot2; TSE systems). The locomotion speed and time together with distance travelled were estimated with the multi-cage locomotion monitor mode.

2.4.5 Visual discrimination task

The apparatus was an isosceles trapezoidal-shaped swimming pool (Prusky et al., 2000) filled with water (15 cm depth). A 50% gray image (non-reinforced stimulus, CS⁻) and a fixed image with a black triangle on the white background (conditioned stimulus, CS⁺) were pinned on the walls of the wider end of the pool. The two images were separated by a black board in the middle so that a mouse cannot see the image on the other side. On the side of the CS⁺ image, a platform was placed beneath the water surface (Figure 5A).

In a visual discrimination task mice were trained to discriminate the CS⁺ and the CS⁻ images by swimming to the CS⁺ image and climbing onto the submerged platform. Each mouse was given three blocks of ten training units per day in five consecutive days. Once a mouse crossed the choice line with more than a half of its body length, it was considered to have made a decision. For a wrong decision the mouse must repeat the trial immediately. In one training unit, a mouse was allowed to make maximum five errors (Figure 5B). To avoid the effect of positional learning, the side of the CS⁺ image and the platform was pseudo-randomly changed after each trial according to a Gellerman schedule (LRLRLRR, L=left, R=right) (Trevino et al., 2013). To assess the visual discrimination capacity, the mean probability of making a correct decision in the first presentation (correct %) per day and the total swimming trials per day were analyzed.

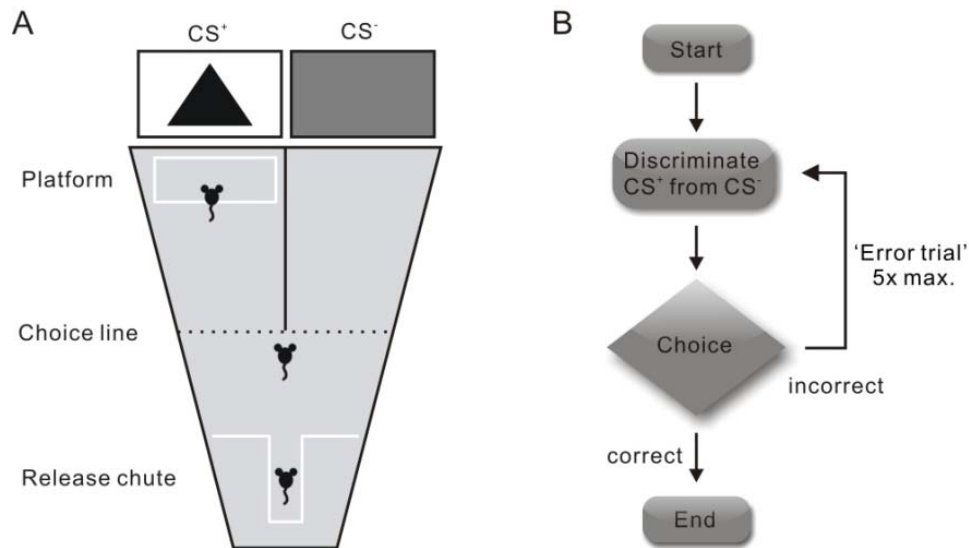


Figure 5: Visual discrimination task. (A) Scheme of the visual discrimination task: Mice were released from the release chute of the Y-shaped maze and learned to swim to the submerged platform indicated by a white rectangle beneath the CS⁺ image. The position of CS⁺ image and platform was pseudo-randomly altered over trials. The mice were considered to have made a choice when half of its body crossed the choice line. (B) Flowchart of a “training unit”. Mice were forced to repeat the trial up to five times if they made a wrong choice.

2.5 EEG measurements

To measure the EEG and EMG traces, a telemetric EEG transmitter (F20-EET, Data Science International) was introduced. The EEG transmitter was in a cylindrical shape with a diameter of 8 mm, a length of 20 mm and a weight of 3.8 g. The transmitter contained four electrodes, each with a length of approximately 3 cm. The telemetric system made it possible to continuously monitor the EEG measurements of the freely moving mice. A stress-free EEG trace recording was attributed to the wireless data transmission, which was critical for the detection of a normal sleeping pattern in mice. The surgery to transplant the EEG transmitters was performed using isoflurane narcosis combined with xylazin and carprofen analgesia. The “Regierung von Oberbayern” proofed all procedures with the official sign code 55.2-1-54-2532-172-11.

The head of a mouse was fixed in a stereotactic apparatus (Fa. TSE-System, Bad Homburg) and the body temperature was maintained constant at 37°C via a rectal feedback control system. By a small (1.5 cm-long) incision, the scalp was first opened along the median of the head and the

skullcap (Cranium cerebrale) was dissected. A second incision was made caudally on the bladebone along the longitudinal axis. With a pair of blunt scissors, a small pocket was created for the transmitter and the two electrodes for electromyography (EMG) were placed on the muscle and fixed with some stiches (Figure 6, left). Two tiny holes were drilled in the skullcap (0.7 mm in diameter) with following co-ordinates: 2 mm posterior to the bregma and 1.8 mm lateral to the sagittal suture on the right side; 1 mm posterior to the lambda and 0.5 mm lateral to the sagittal on the left side (Figure 6, right) (Paxinos and Franklin, 2008). The two electrodes for EEG were placed into the holes and fixed with acryl cement. After that, the scalp was closed with some stiches.

After a two-week recovery, the cortical EEG and EMG traces of the freely moving mice were recorded with the DSI A.R.T. software. The data was analyzed with Neuroscore2.1 (Data Science International) and processed in GraphPad Prism5. The EEG measurement was performed by Dr. Verena Hammelmann and Saskia Spahn in our laboratory.

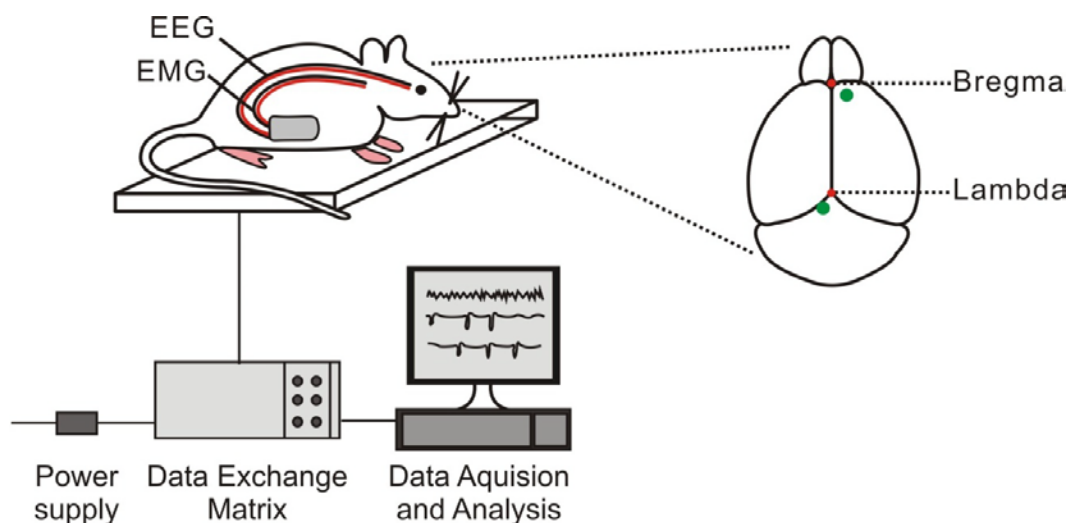


Figure 6: *In vivo* EEG measurement. Mice were transplanted with a telemetric EEG transmitter to record the EEG traces and the EMG signals (left). The exact location of the two holes for EEG electrodes was indicated by green circles, bregma and lambda were indicated by red circles (right).

2.6 Optical coherence tomography (OCT)

The ophthalmic examinations of the mouse retinas were performed using the Micron IV system (Phoenix research labs, Pleasanton, United States). For this purpose, mice were anesthetized with an intraperitoneal injection of ketamin (0.1 mg/g) and xylazin (0.02 mg/g). Dilation of their pupils was achieved by adding one drop of Tropicamid eye (Mydriadicum Stulln, Pharma Stulln GmbH, Germany). Subsequently, retinal OCT images were taken of the anaesthetized mice. During the examination, hydroxypropyl methylcellulose (Methocel 2%; OmniVision, Puchheim, Germany) kept the eyes moist. Retinal thickness was measured in the dorsal part of the retina. The OCT measurement was performed by Dr. Christian Schön in our laboratory.

2.7 Statistical analysis

Data were presented as mean \pm SEM and analyzed with two-way ANOVA followed by a post-hoc Bonferroni test or Student *t* test followed by a Mann-Whitney *u* test using the Origin (Northampton, MA) or GraphPad Prism software (San Diego, CA).

3. Results

3.1 Generating HCN2-1 switch mice

HCN2-1 switch mice possess a mixed C57BL/6J genetic background. The HCN2-1 heterozygous mice (HCN2^{+/sw}) were mated to produce HCN2-1 homozygous (SW, HCN2^{sw/sw}) and wild-type mice (WT, HCN2^{+/+}). The WT and the homozygous HCN2-1 switch allele showed a fragment of 316 bp and 414 bp, respectively (Figure 7).

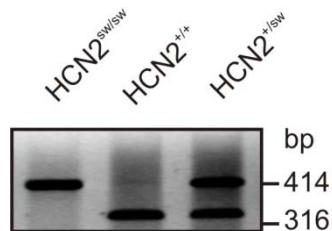


Figure 7: Multiplex PCR analysis of genomic DNA in HCN2^{+/+}, HCN2^{sw/sw} and HCN2^{+/sw} mice. A 316 bp product from HCN2^{+/+} and a 414 bp product from HCN2^{sw/sw} were given. HCN2^{+/sw} showed a combination of both bands.

3.2 Biochemical analyses of HCN2-1 switch mice

In HCN2^{sw/sw} mice, the replacement of exon 1 in the *HCN2* gene by a coding region of mHCN1 was confirmed at DNA level by southern blot analysis (previously done by Christian Grunner in our labotory). To determine the transcription of FLAG-HCN1 mRNA instead of HCN2 mRNA, northern blot analysis, *in situ* hybridization and quantitative PCR were performed. Furthermore, the expression of FLAG-HCN1 protein and the absence of HCN2 protein expression in HCN2^{sw/sw} mice were confirmed by western blot analysis and immunohistochemistry. The brain morphology of HCN2^{sw/sw} mice was examined by the Nissl staining.

3.2.1 Absence of HCN2 mRNA in HCN2^{sw/sw} mice

A specific probe corresponding to the amino acids 176-378 of mHCN2 (Ludwig et al., 2003) was hybridized with the blot containing polyA⁺ mRNAs from the brains of WT, HCN2^{sw/sw} and HCN2^{-/-} mice. The mHCN2 mRNA was detected in WT mice and represented by a 3.4-kb band, but absent in HCN2^{sw/sw} and HCN2^{-/-} mice (Figure 8A). With a specific probe corresponding to the amino acids 332-396 of mHCN1, the multiple HCN1 transcripts (at 8.3 kb, 4.4 kb, 3.8 kb and 3.4 kb) were detected, among which the 3.4 kb band concurred with the predicted HCN1 cDNA in size (Figure 8B) (Santoro et al., 1997; Ludwig et al., 1998). The glyceraldehyde 3-phosphate dehydrogenase (GAPDH) mRNA served as an internal loading control.

The distribution patterns of HCN1 and HCN2 mRNA in WT and HCN2^{sw/sw} mice were determined by *in situ* hybridization. The brain sections were hybridized with single-stranded antisense RNA probes that share the same target sequences with the probes for northern blot. HCN2 mRNAs were expressed abundantly throughout the WT brain with the highest signal in the thalamus and brainstem (Figure 8C, upper left), whereas no HCN2 mRNA was detected in HCN2^{sw/sw} mice (Figure 8C, upper right). HCN1 mRNAs in WT mice were mainly distributed in the cortex, hippocampus and cerebellum (Figure 8, lower left). A similar distribution pattern of the HCN1 mRNAs in HCN2^{sw/sw} mice was observed (Figure 8C, lower right). The results confirmed that the HCN2 mRNA was not transcribed in HCN2^{sw/sw} mice. Theoretically HCN1 mRNA in HCN2^{sw/sw} mice would display a combined distribution pattern of both HCN1 and HCN2 mRNA from WT mice, however, the results suggested otherwise. We hypothesize that FLAG-HCN1 mRNA would be transcribed at a lower level compared to the endogenous HCN1 and HCN2 transcripts. To further dissect the endogenous HCN1 and FLAG-HCN1 mRNA, we performed *in situ* hybridization with a FLAG probe (69 bp) as described above. Still no signal was detected in HCN2^{sw/sw} mice (data not shown). It is possible that the FLAG probe is too short as suggested that the probe for *in situ* hybridization should be at least 100 bp.

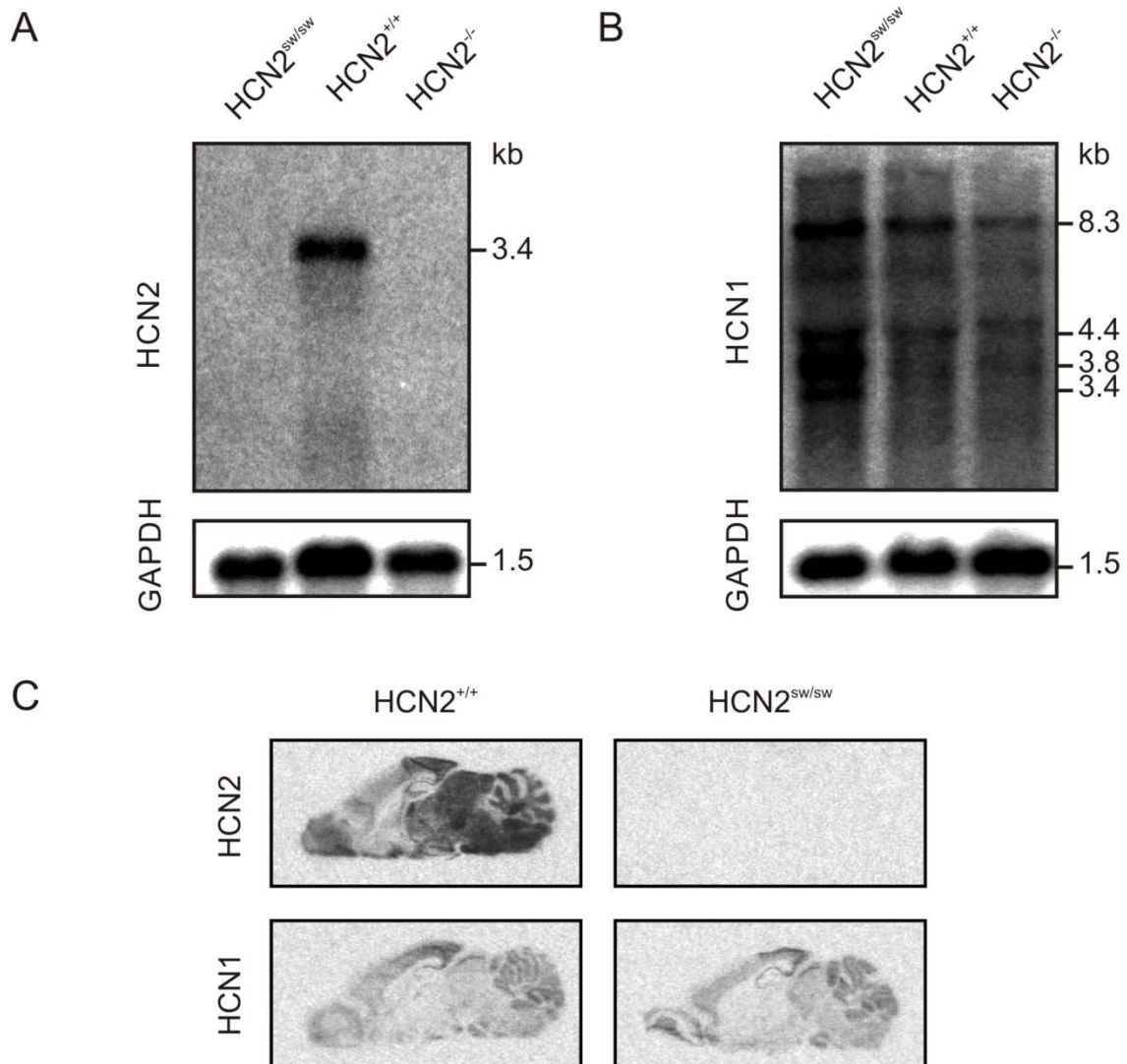


Figure 8: Analysis of mRNA expression in HCN2^{+/+}, HCN2^{sw/sw} and HCN2^{-/-} mice. (A and B) Northern blot analysis of polyA⁺ mRNA from the mouse brains hybridized with ³²P-labeled HCN2 (A, top) or HCN1 probes (B, top). GAPDH served as loading control (A and B, bottom). Coronal brain sections were *in situ* hybridized with antisense ³⁵S-labeled probes against HCN2 (top panels) or HCN1 (bottom panels) mRNA.

3.2.2 Expression of FLAG-HCN1 mRNA in HCN2^{sw/sw} mice

In order to confirm the FLAG-HCN1 transcription in HCN2^{sw/sw} mice, quantitative PCR was performed. Using primers spanning the exons 3 and 4 of HCN1, the amount of HCN1 mRNAs in the brain of WT, HCN2^{sw/sw}, HCN2^{-/-} and HCN1^{-/-}/HCN2^{sw/sw} mice at three postnatal stages (P1, P10 and P42) was quantified. The HCN1 mRNA in WT at P1 was set as 1.00. All relative mRNA expression data were summarized in Table 2 and Figure 9 (A and B).

The quantity of HCN1 mRNAs in the brain of HCN2^{sw/sw} mice was significantly increased compared to the age-matched WT mice. The increase was 48% at P1 ($p=0.0127$), 20% at P10 ($p=0.0106$) and 30% at P42 ($p=0.0125$), respectively (Figure 9A; Table 2). In HCN2-deficient mice, the expression of HCN1 was not affected (Figure 9A; Table 2), suggesting that deletion of *HCN2* gene did not result in an upregulation in HCN1 mRNA. Therefore, such an increase in HCN2^{sw/sw} mice should be caused by the FLAG-HCN1 mRNA. The FLAG-HCN1 transcription was further confirmed in HCN1^{-/-}/HCN2^{sw/sw} mice, in which the endogenous HCN1 was deleted and HCN2 was replaced by FLAG-HCN1. The HCN1 mRNA detected in these mice represented only FLAG-HCN1. Indeed, HCN1 mRNA was transcribed at a low level (Figure 9A; Table 2). Due to their short lifespan (maximum 13 days), the P42 data for HCN1^{-/-}/HCN2^{sw/sw} mice was not obtained. These results indicated that FLAG-HCN1 mRNA was transcribed in HCN2^{sw/sw} mice.

Table 2. Relative expression level of HCN1 and HCN2 mRNA

Genotype	HCN1 mRNA			HCN2 mRNA		
	P1	P10	P42	P1	P10	P42
HCN2 ^{+/+}	1.00 ± 0.01	1.86 ± 0.03	2.15 ± 0.03	0.58 ± 0.02	0.84 ± 0.01	1.33 ± 0.05
HCN2 ^{sw/sw}	1.48 ± 0.11	2.22 ± 0.07	2.77 ± 0.14	-	-	-
HCN1 ^{-/-} / HCN2 ^{sw/sw}	0.42 ± 0.01	1.11 ± 0.25	-	-	-	-
HCN2 ^{-/-}	1.09 ± 0.07	1.82 ± 0.11	2.29 ± 0.27	-	-	-

Data were presented as Mean ± SEM. -: data were not obtained.

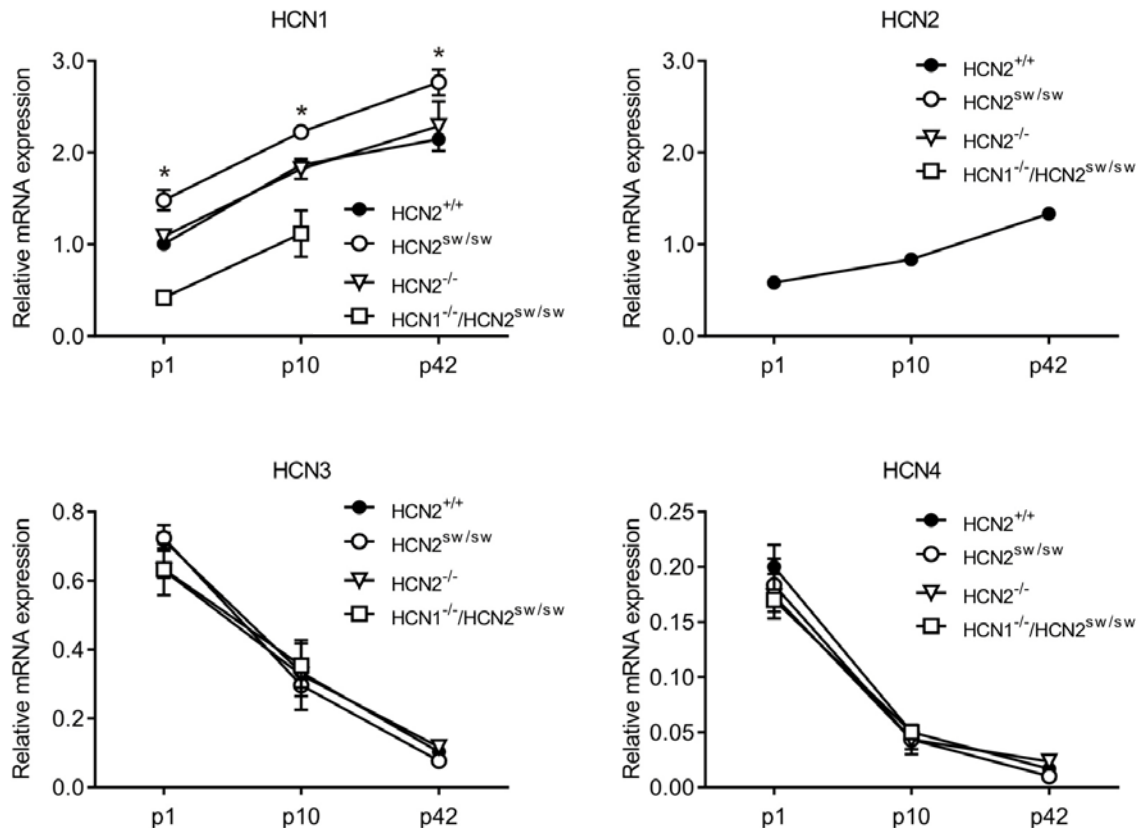


Figure 9: Quantitative analysis of HCN1-4 mRNA expression in the brains of $HCN2^{+/+}$, $HCN2^{sw/sw}$, $HCN2^{-/-}$ and $HCN1^{-/-}/HCN2^{sw/sw}$ mice. Relative HCN1 (A), HCN2 (B), HCN3 (C) and HCN4 (D) mRNA expression levels in the brains of $HCN2^{+/+}$ (●), $HCN2^{sw/sw}$ (○), $HCN2^{-/-}$ (△) and $HCN1^{-/-}/HCN2^{sw/sw}$ (□) mice were plotted as a function of age. The HCN1 mRNA in WT at P1 was set as 1.00. Data were presented as mean \pm SEM. $n=3$. Post-hoc Tukey test followed by one-way ANOVA. (A, * $p<0.05$ between $HCN2^{+/+}$ and $HCN2^{sw/sw}$ mice).

HCN2 mRNA can be detected only in WT mice. Its expression level was 58% of HCN1 mRNA at P1, 45% at P10 and 61% at P42, respectively (Figure 9B; Table 2). Notably, the expression level of HCN1 in $HCN1^{-/-}/HCN2^{sw/sw}$ mice was comparable to that of HCN2 mRNA in the age-matched WT mice. Moreover, the combined level of HCN1 and HCN2 mRNA in WT mice were comparable to the level of total HCN1 mRNA in the age-matched $HCN2^{sw/sw}$ mice, suggesting that FLAG-HCN1 was transcribed under the control of the HCN2 promoter.

3.2.3 Unaltered HCN3 and HCN4 expression levels in HCN2^{sw/sw} mice

Quantitative analyses revealed that neither deletion of *HCN2* gene nor replacement of *HCN2* gene with *HCN1* gene affected the expression of HCN3 and HCN4 mRNA (Figure 9C and D; Table 3).

Additionally, a progressive increase in total HCN1 and HCN2 mRNA was detected in the brains of WT, HCN2^{sw/sw}, HCN2^{-/-} and HCN1^{-/-}/HCN2^{sw/sw} mice as a function of age, whereas expression levels of HCN3 and HCN4 mRNAs decreased over age (Figure 9; Table 2 and 3).

Table 3. Relative expression level of HCN3 and HCN4 mRNA

Genotype	HCN3 mRNA			HCN4 mRNA		
	P1	P10	P42	P1	P10	P42
HCN2 ^{+/+}	0.72 ± 0.02	0.33 ± 0.02	0.10 ± 0.01	0.20 ± 0.02	0.05 ± 0.01	0.02 ± 0.003
HCN2 ^{sw/sw}	0.72 ± 0.04	0.30 ± 0.03	0.08 ± 0.01	0.18 ± 0.02	0.05 ± 0.01	0.01 ± 0.001
HCN1 ^{-/-} / HCN2 ^{sw/sw}	0.63 ± 0.02	0.35 ± 0.06	-	0.17 ± 0.01	0.05 ± 0.01	-
HCN2 ^{-/-}	0.63 ± 0.08	0.33 ± 0.10	0.12 ± 0.11	0.17 ± 0.02	0.04 ± 0.01	0.02 ± 0.003

Data were presented as Mean ± SEM. -: data were not obtained.

3.2.4 Regional expression pattern of FLAG-HCN1 mRNA in HCN2^{sw/sw} mice

Considering the distinct regional distribution patterns of HCN mRNAs in the mouse brain (Santoro et al., 2000), the expression of HCN1-4 in the four brain regions, i.e. hippocampus, cortex, thalamus and substantia nigra (SN) was determined using quantitative PCR in WT, HCN2^{sw/sw} and HCN2^{-/-} mice at P42. In each region, the expression level of HCN1 in WT mice was set as 1.00. The relative mRNA expression levels were summarized in Figure 10 and Table 4-7.

Table 4. Relative expression levels of HCN1-HCN4 mRNA in hippocampus of P42-old mice

Genotype	Hippocampus			
	HCN1	HCN2	HCN3	HCN4
HCN2 ^{+/+}	1.00 ± 0.02	0.33 ± 0.01	0.04 ± 0.01	< 0.002
HCN2 ^{sw/sw}	1.24 ± 0.03	-	0.04 ± 0.01	< 0.002
HCN2 ^{-/-}	1.14 ± 0.02	-	0.03 ± 0.01	< 0.002

Data were presented as Mean ± SEM. -: data were not obtained.

Table 5. Relative expression levels of HCN1-HCN4 mRNA in cerebellum of P42-old mice

Genotype	Cerebellum			
	HCN1	HCN2	HCN3	HCN4
HCN2 ^{+/+}	1.00 ± 0.04	0.25 ± 0.01	0.02 ± 0.001	< 0.002
HCN2 ^{sw/sw}	1.29 ± 0.07	-	0.02 ± 0.001	< 0.002
HCN2 ^{-/-}	1.09 ± 0.02	-	0.02 ± 0.001	< 0.002

Data were presented as Mean ± SEM. -: data were not obtained.

Table 6. Relative expression levels of HCN1-HCN4 mRNA in thalamus of P42-old mice

Genotype	Thalamus			
	HCN1	HCN2	HCN3	HCN4
HCN2 ^{+/+}	1.00 ± 0.05	2.23 ± 0.55	0.35 ± 0.05	0.20 ± 0.14
HCN2 ^{sw/sw}	2.66 ± 0.23	-	0.42 ± 0.05	0.17 ± 0.05
HCN2 ^{-/-}	1.77 ± 0.29	-	0.34 ± 0.02	0.13 ± 0.08

Data were presented as Mean ± SEM. -: data were not obtained.

Table 7. Relative expression levels of HCN1-HCN4 mRNA in substantia nigra of P42-old mice

Genotype	Substantia nigra			
	HCN1	HCN2	HCN3	HCN4
HCN2 ^{+/+}	1.00 ± 0.07	1.32 ± 0.14	0.16 ± 0.03	0.02 ± 0.005
HCN2 ^{sw/sw}	2.09 ± 0.21	-	0.16 ± 0.02	0.03 ± 0.006
HCN2 ^{-/-}	1.42 ± 0.18	-	0.18 ± 0.05	0.03 ± 0.006

Data were presented as Mean ± SEM. -: data were not obtained.

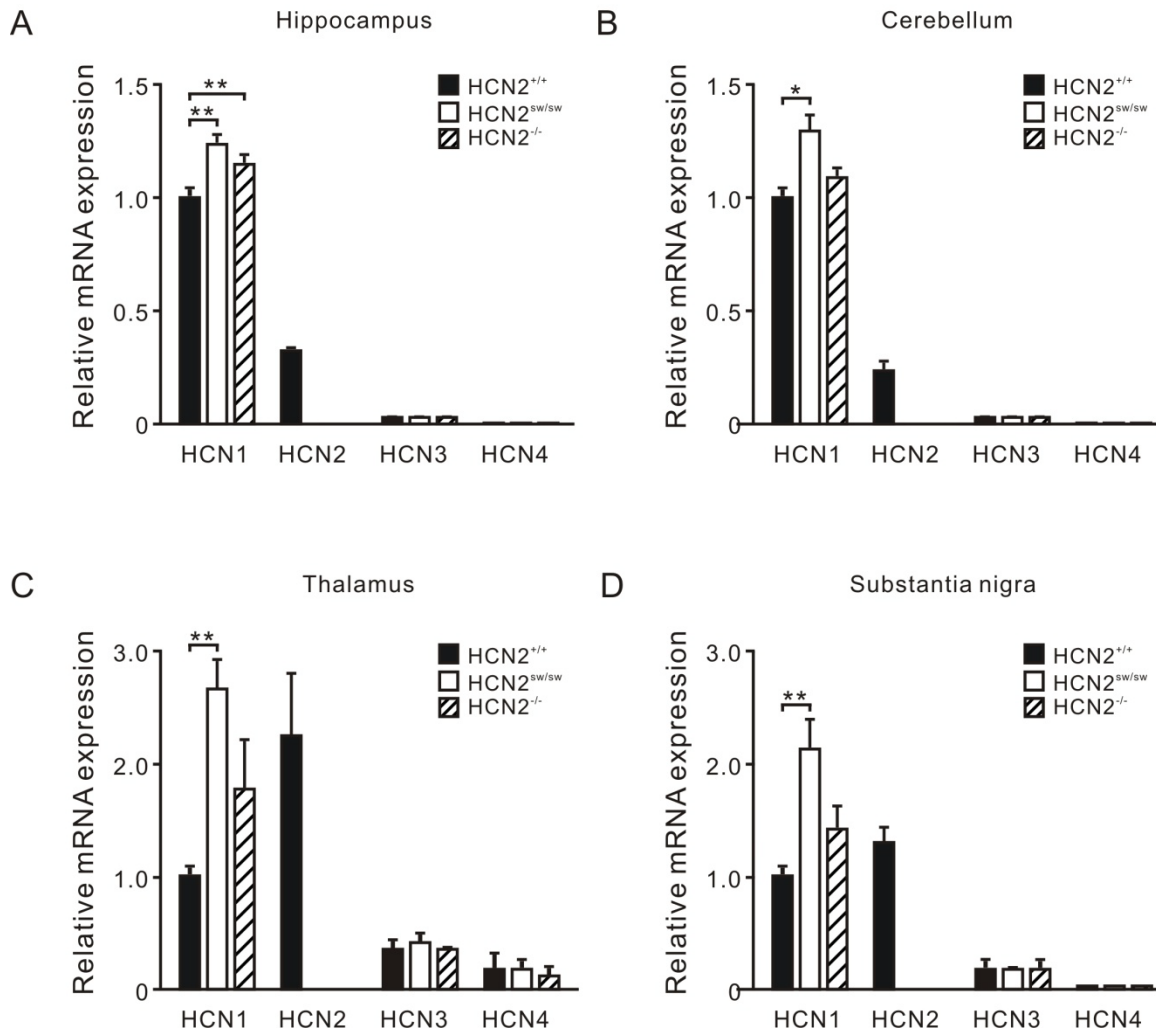


Figure 10: Quantitative analysis of HCN1-4 mRNA expression in four brain regions of HCN2^{+/+}, HCN2^{sw/sw} and HCN2^{-/-} mice at P42. The relative expression levels of HCN1-4 mRNAs in the hippocampus (A), cerebellum (B), thalamus (C) and substantia nigra (D) were determined by qPCR. The HCN1 in WT mice in each brain region was set as 1.00, respectively. HCN2^{+/+}, solid bar; HCN2^{sw/sw}, open bar; HCN2^{-/-}, hatched bar. Data were presented as mean \pm SEM. n=3. * p<0.05, ** p<0.01. Post-hoc Tukey test followed by one-way ANOVA.

In WT mice, HCN1 mRNA was more abundant than HCN2 mRNA in hippocampus and cerebellum (3-fold in hippocampus, $p < 0.0001$; 4-fold in cerebellum, $p < 0.0001$) (Figure 10A and B; Tables 4 and 5). By contrast, HCN2 mRNA was more than HCN1 in the thalamus and SN (2.23-fold in thalamus, $p = 0.0883$; 1.32-fold in SN, $p = 0.0982$) (Figure 10C and D; Tables 6 and 7). These results were in consistency with previous publications (Moosmang et al., 1999; Santoro et al., 2000; Notomi and Shigemoto, 2004). Compared to WT, the amount of HCN1 mRNA in HCN2^{sw/sw} mice was increased 25% in hippocampus ($p = 0.0022$; Figure 10A, Table 4), 29% in cerebellum

($p=0.0121$; Figure 10B, Table 5), 166% in thalamus ($p=0.0883$; Figure 10C, Table 6) and 109% in SN ($p=0.0982$; Figure 10D, Table 7). In the four brain regions except hippocampus, the expression level of HCN1 mRNA remained unaltered in HCN2^{-/-} mice (Figure 10; Table 4-7). These results suggested that the regional expression pattern of the FLAG-HCN1 mRNA in HCN2^{sw/sw} mice was in line with that of HCN2 in WT.

Compared to WT mice, the expression levels of HCN3 and HCN4 mRNA in the four brain regions remained unchanged in HCN2^{sw/sw} and HCN2^{-/-} mice (Figure 10; Table 4-7).

3.2.5 Expression of FLAG-HCN1 proteins in HCN2^{sw/sw} mice

Since the anti-HCN1 antibody (Abcam) recognizes the C-terminus of HCN1, which is shared by both HCN1 and FLAG-HCN1 proteins, an anti-FLAG M2 antibody (Sigma) was used to detect the FLAG-HCN1 proteins specifically. Western blot analysis of brain membrane protein lysates obtained from various mice revealed that HCN1 and HCN2 but not FLAG-HCN1 proteins were detected in WT mice (Figure 11A, HCN2^{+/+}). In HCN2^{sw/sw} mice, endogenous HCN1 and FLAG-HCN1 but not HCN2 proteins were detected. Although there was an increase in molecular weight (10 kDa) caused by the FLAG tag, yet it was impossible to distinguish the two bands at 130kDa with the anti-HCN1 antibody (Figure 11A, HCN2^{sw/sw}). The HCN2^{+/sw} mice contained a WT allele and an HCN2-1 switch allele; therefore, they showed both HCN2 and FLAG-HCN1 proteins (Figure 11A, HCN2^{+/sw}). Protein lysates from HCN1^{-/-} and HCN2^{-/-} mice were used to display the specificity of anti-HCN1 and anti-HCN2 antibodies (Figure 11A, HCN1^{-/-} and HCN2^{-/-}). The membrane-standing ATPase was used as an internal control to ensure equal loading (Figure 11A, lowest panel).

In the investigations of mouse brain regions, SN was of particular interest, because the nigral dopaminergic neurons express HCN2 but not HCN1 channel subunits (Franz et al., 2000). SN were dissected from the mouse brain as described by Fath et al. (2009). Tyrosine hydroxylase (TH), a neuronal marker for the dopaminergic neurons, was used as an internal control to ensure the regional specificity and equal loading in western blot analysis (Figure 11B, the lowest panel). As shown in Figure 11B, FLAG-HCN1 could only be detected in HCN2^{sw/sw} mice, but not in WT and HCN2^{-/-} mice, whereas HCN2 was only detected in WT mice. Generally, newly generated FLAG-

HCN1 proteins were detectable in various regions throughout the CNS of HCN2^{sw/sw} mice (Figure 11C).

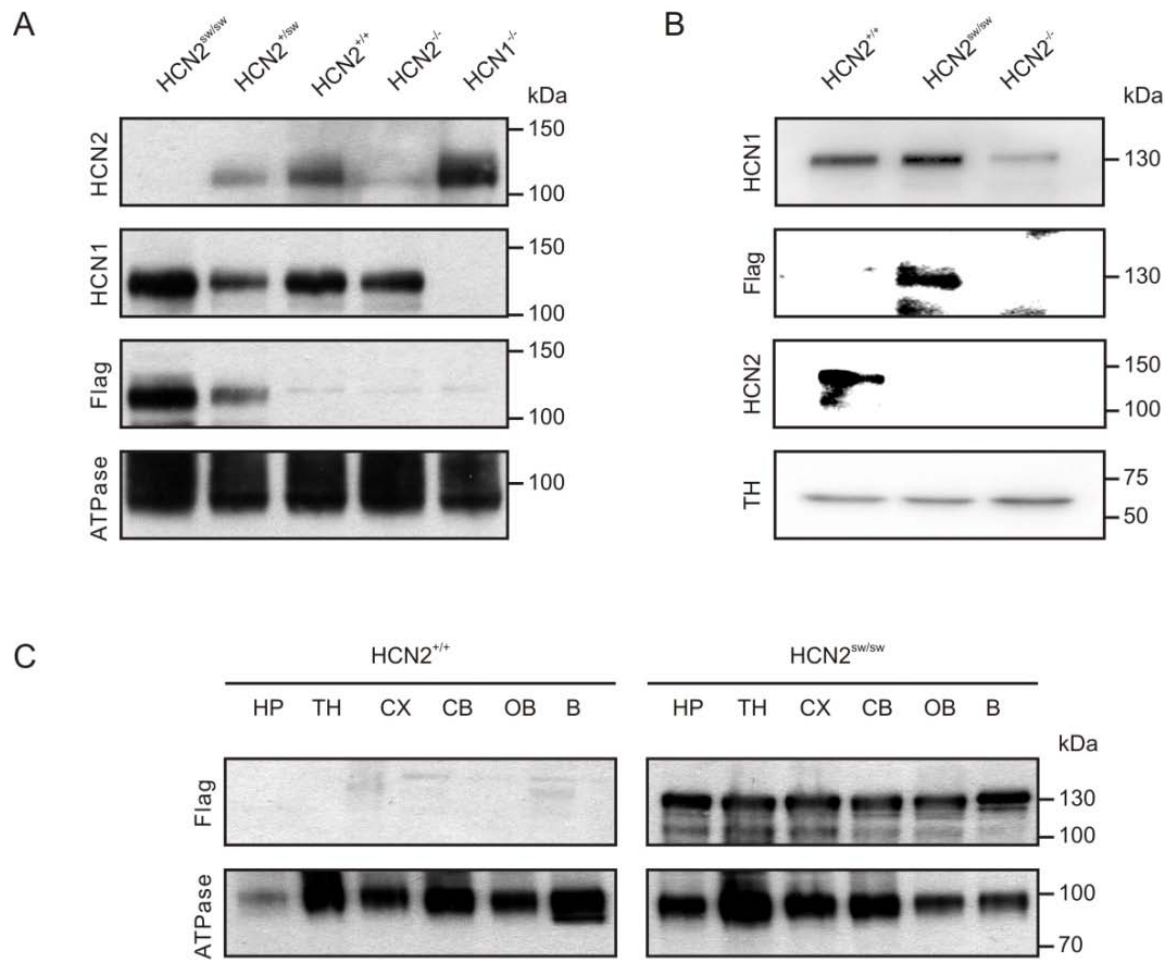


Figure 11: Western blot analysis of FLAG-HCN1 expression in mouse brains. (A) Immunoblots of membrane proteins from the whole brain lysates of HCN2^{+/+}, HCN2^{sw/sw}, HCN2^{+/sw}, HCN1^{-/-} and HCN2^{-/-} mice aged 6-8 weeks. ATPase served as a loading control for membrane proteins. (B) Immunoblots of membrane proteins from the SN of HCN2^{+/+}, HCN2^{sw/sw} and HCN2^{-/-} mice aged 6-8 weeks. Tyrosine hydroxylase (TH) indicated the regional specificity. (C) Immunoblots of membrane proteins from five brain regions of HCN2^{+/+} and HCN2^{sw/sw} mice aged 6-8 weeks. The whole brain lysate served as positive control. HP: hippocampus, TH: thalamus, CX: cortex, CB: cerebellum, OB: olfactory bulb, B: whole brain lysate.

3.2.6 Glycosylation of FLAG-HCN1 proteins

Mammalian HCN channels in the brain are N-linked glycosylated. Glycosylation is crucial for the membrane trafficking and the functional expression of HCN channels (Much et al., 2003). Therefore, the glycosylation of FLAG-HCN1 proteins was investigated using PNGase F which removes the high mannose, hybrid, and complex *N*-glycans from the glycoproteins, resulting in a reduced molecular weight.

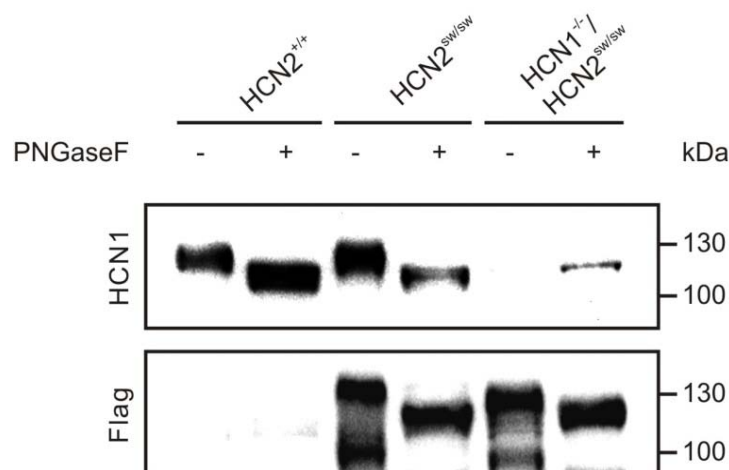


Figure 12: Deglycosylation assay of FLAG-HCN1 protein. 30 μ g of membrane proteins from the mouse brain of WT, HCN2^{sw/sw} and HCN1^{-/-}/HCN2^{sw/sw} mice aged 6-8 weeks were treated (+) or untreated (-) with PNGase F followed by detection with anti-HCN1 (upper panel) and anti-FLAG antibody (lower panel).

Deglycosylation reduced the molecular weight of WT HCN1 proteins from 130 to 120 kDa (Figure 12, upper panel, HCN2^{+/+}). This was in accordance with the theoretical molecular mass of HCN1. A similar migration pattern of HCN1 proteins was observed in HCN2^{sw/sw} (Figure 12, upper panel, HCN2^{sw/sw}). The untreated FLAG-HCN1 proteins in HCN1^{-/-}/HCN2^{sw/sw} mice were not detected with the anti-HCN1 antibody probably due to their low expression level (Figure 12, upper panel, HCN1^{-/-}/HCN2^{sw/sw}). To specifically detect the FLAG-HCN1, the same blot was restriped and then incubated with the anti-FLAG M2 antibody. As expected, no FLAG-protein was detected in the WT mice (Figure 12, lower panel, HCN2^{+/+}). In HCN2^{sw/sw} mice, the untreated and treated deglycosylated FLAG-HCN1 were observed at about 135 and 119 kDa, respectively (Figure 12, lower panel, HCN2^{sw/sw}). This indicated that FLAG-HCN1 proteins were glycosylated *in vivo*. The untreated FLAG-HCN1 proteins in HCN1^{-/-}/HCN2^{sw/sw} mice had the molecular weight of 124 kDa,

lower than the molecular weight of FLAG-HCN1 in HCN2^{sw/sw} mice (135 kDa), however, the deglycosylated FLAG-HCN1 proteins in these two mice had same molecular weights (Figure 12, lower panel, HCN1^{-/-}/HCN2^{sw/sw}). We speculated that the FLAG-HCN1 proteins in HCN1^{-/-}/HCN2^{sw/sw} mice had undergone an incomplete glycosylation process.

3.2.7 Immunohistochemistry analysis of FLAG-HCN1 distribution in HCN2^{sw/sw} mice

We analyzed the distribution pattern of the total HCN1, including endogenous HCN1 and FLAG-HCN1, in HCN2^{sw/sw} mice using anti-HCN1 antibody (Alomone), which recognizes the N-terminus of HCN1 protein. The reason that we did not use anti-FLAG antibodies was that they generated unspecific stainings in the WT sections. The immunohistochemical analyses revealed that the FLAG-HCN1 proteins in HCN2^{sw/sw} mice were expressed in the same pattern as the HCN2 proteins in WT mice.

Epifluorescent images were taken from four brain regions of WT and HCN2^{sw/sw} mice (CA1, CA2/3, thalamus and cerebellum) aged 6-8 weeks. Both WT and HCN2^{sw/sw} mice exhibited similar HCN1 expression in the stratum lacunosum-moleculare (slm) of hippocampal CA1 region and in the cerebellar Purkinje cell layer (Figure 13A, CA1 and CB), suggesting that FLAG-HCN1 was expressed at low level in these regions. However, the HCN1 intensity in the thalamus was largely increased in HCN2^{sw/sw} mice (Figure 13A, TH), implicating that the FLAG-HCN1 proteins were expressed at a high level. These observations were in consistence with the mRNA expression levels determined by qPCR analysis, in which the difference in HCN1 mRNA expression level between WT and HCN2^{sw/sw} mice in the thalamus was more profound than that in the hippocampus and cerebellum (Chapter 3.2.4).

HCN2 proteins were abundantly expressed in the thalamus (Figure 13B, HCN2^{+/+}, TH) and moderately in the slm of CA1 region (Figure 13B, HCN2^{+/+}, CA1), in the interneuron of CA2/CA3 regions (Figure 13B, HCN2^{+/+} CA2/CA3) as well as in the cerebellar granule layer of WT mice (Figure 13B, HCN2^{+/+}, CB).

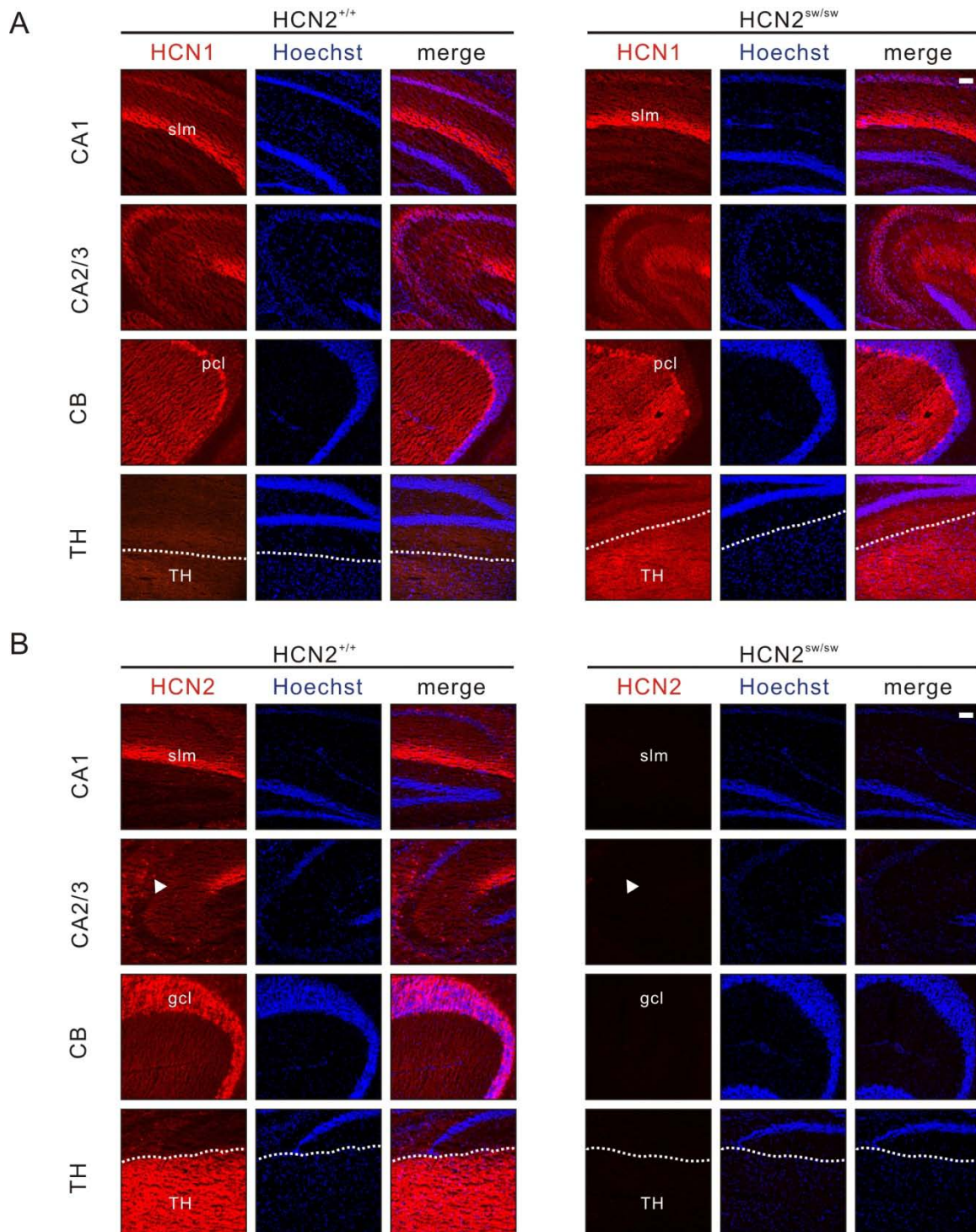


Figure 13: Immunohistochemical analysis of HCN1 and HCN2 proteins in four brain regions of HCN2^{+/+} and HCN2^{sw/sw} mice aged 6-8 weeks. Epifluorescent images of the distribution of HCN1 (red in A) and HCN2 (red in B) in CA1, CA2/CA3, cerebellum and thalamus. Cell nuclei were counterstained with Hoechst (blue). Arrowhead indicated the interneurons in the CA2/CA3 region. slm: stratum lacunosum-moleculare, pcl: Purkinje cell layer, gcl: granule cell layer, TH: thalamus. Scale bar: 100 μ m.

In contrast, no HCN2 proteins were detected in any of the brain regions of HCN2^{sw/sw} mice (Figure 13B, HCN2^{sw/sw}), which was consistent with the results from the western blot analysis (Chapter 3.2.4).

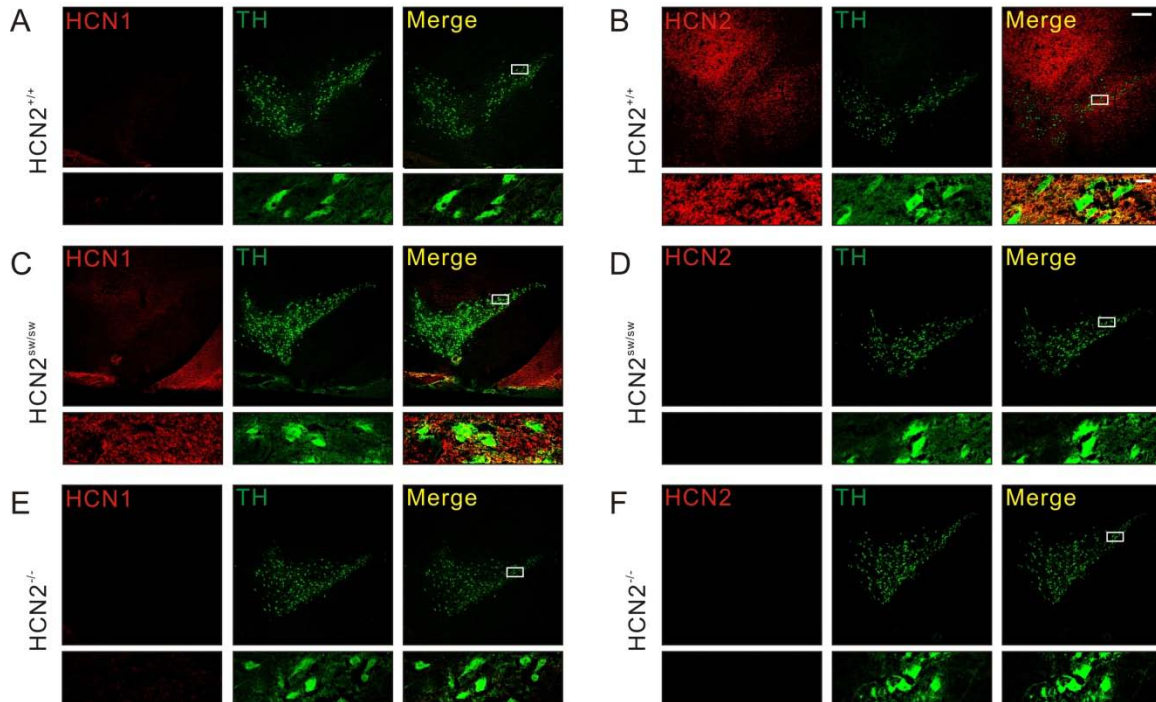


Figure 14: Immunohistochemical characterization of HCN1 and HCN2 in the SN of HCN2^{+/+}, HCN2^{sw/sw} and HCN2^{-/-} mice aged 6-8 weeks. Coronal brain sections were stained for HCN1 (red in A, C and E), HCN2 (red in B, D and F) and tyrosine hydroxylase (green). The upper panels were confocal images of the area of SN and ventral tegmental area (scale bar: 100 μ m). The lower panels were the area demarcated by the white boxes in upper panels at higher magnification (scale bar: 10 μ m). TH: tyrosine-hydroxylase.

A special focus was placed on the substantia nigra pars compacta (SNc). The SN and VTA were identified by a crescent shape (Figure 14, upper panels, green). Dopaminergic neurons in the SNc were magnified to show the staining of the cytosolic TH and the membrane-localized HCN channels (Figure 14, lower panels). In WT dopaminergic neurons, HCN2 but not HCN1 was detected (Figure 14A and B), which was in consistency with the results of Franz et al. (2000). In SW dopaminergic neurons, HCN1 but not HCN2 was detected (Figure 14C and D). In contrast to both of them, the HCN2-deficient dopaminergic neurons exhibited negative staining in both HCN1 and HCN2 (Figure 14E and F).

3.3 Normal brain morphology in HCN2^{sw/sw} mice

A nissl staining with cresyl-violet revealed the normal brain morphology in the HCN2^{sw/sw} mice. In comparison with the WT sections, the typical brain structures remained unchanged in the HCN2^{sw/sw} sections, like striatum and globus pallidus (GP) in the forebrain (Figure 15, 1), CA1-3 regions and dentate gyrus (Figure 15, 2), thalamus (Figure 15, 3), dark labeled SN (Figure 15, 4) and cerebellum (Figure 15, 5).

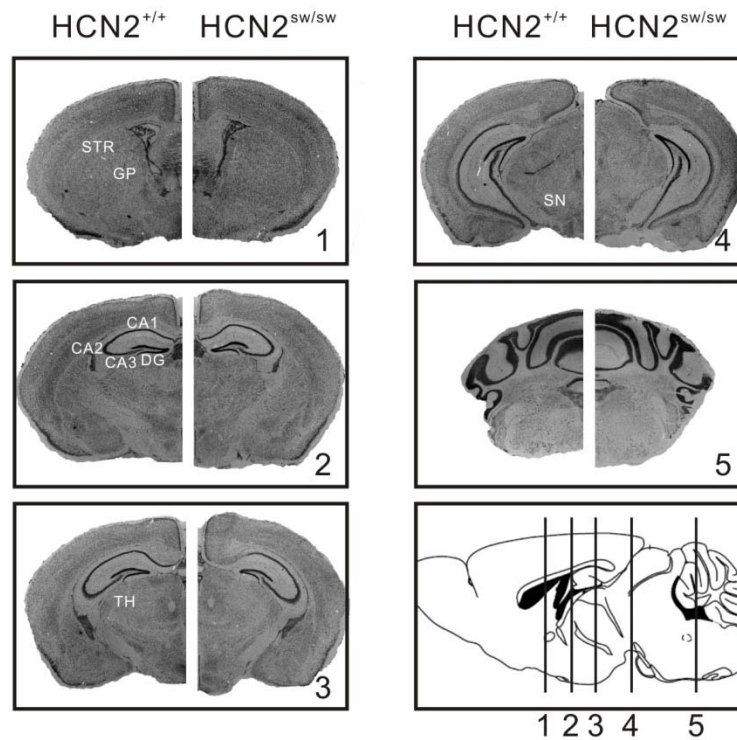


Figure 15: Brain morphology of HCN2^{+/+} and HCN2^{sw/sw} mice aged 6-8 weeks. Coronal sections were stained with cresyl-violet. Representative images of forebrain (1), hippocampus (2), thalamus (3), SN (4, arrow) and cerebellum (5). Numbers indicated the location of each brain region in a sagittal image from the mouse brain atlas. STR: striatum, GP: globus pallidus, CA: cornu amonis, DG: dentate gyrus, TH: thalamus, SN substantia nigra.

3.4 Behavioral tests of HCN2-1 switch mice

As HCN2^{sw/sw} mice grew, dwarfism and ataxia became apparent. In addition, HCN2^{sw/sw} mice displayed wobbling, hind leg splaying, belly dragging, fewer rearing, loss of muscle strength and whole-body tremors, but to a less severe extent than HCN2-deficient mice (Figure 16A). Moreover, HCN2^{sw/sw} mice can normally feed themselves by standing with their hind legs while HCN2-deficient mice failed. To identify different phenotypes among WT, HCN2^{sw/sw} and HCN2-deficient mice, we analyzed them in body growth assessments, longevity study and behavioral tests. Because HCN2^{sw/sw} and HCN2-deficient mice have different genetic backgrounds, each of them was compared to their own WT littermates. In the chapter 3.4.1, 3.4.2 and 3.4.3, the WT littermates of the HCN2^{sw/sw} mice were defined as HCN2^{+/+}(●) to distinguish the WT littermates of the HCN2-deficient mice defined as HCN2^{+/+}(▲).

3.4.1 Reduced body size and shortened lifespan in HCN2^{sw/sw} mice

Adult HCN2^{sw/sw} and HCN2-deficient mice can be easily distinguished from their own WT littermates by diminished body length (HCN2^{+/+}(●): 10.54 ± 0.08 cm, HCN2^{sw/sw}: 9.05 ± 0.12 cm, p<0.0001; HCN2^{+/+}(▲): 10.17 ± 0.06 cm, HCN2^{-/-}: 6.81 ± 0.18 cm, p<0.0001) (Figure 16B). HCN2^{sw/sw} mice have a longer body length than HCN2-deficient mice (p<0.0001).

The body weights of the animals were plotted as a function of age. Normal WT mice gained weight till a plateau at about eight months (Figure 16C). HCN2^{sw/sw} mice grew rapidly in the first three months, after that their body weights kept relatively stable (Figure 16C). The average weight of HCN2^{sw/sw} mice at eight months was approximate 65% of their WT littermates at the same age (HCN2^{+/+}(●): 39.56 ± 2.64 g; HCN2^{sw/sw}: 22.06 ± 0.62 g). HCN2-null mice had a low body weight and showed a rapid and acute deterioration in the health status after five months (Figure 16C, HCN2^{+/+}(▲): 32.33 ± 0.77 g; HCN2^{-/-}: 14.13 ± 2.81 g).

In order to determine the survival rate of WT, HCN2^{sw/sw} and HCN2-deficient mice during a period of 20 months, they were maintained in single cages and supplied with food and water *ad libitum*. After six to seven months 50% of HCN2^{sw/sw} mice died spontaneously, and the remaining 50% survived for as long as 14 months (Figure 16D). 40% of HCN2-null mice died within the first month after birth and the other 60% died successively within eight months (Figure 16D).

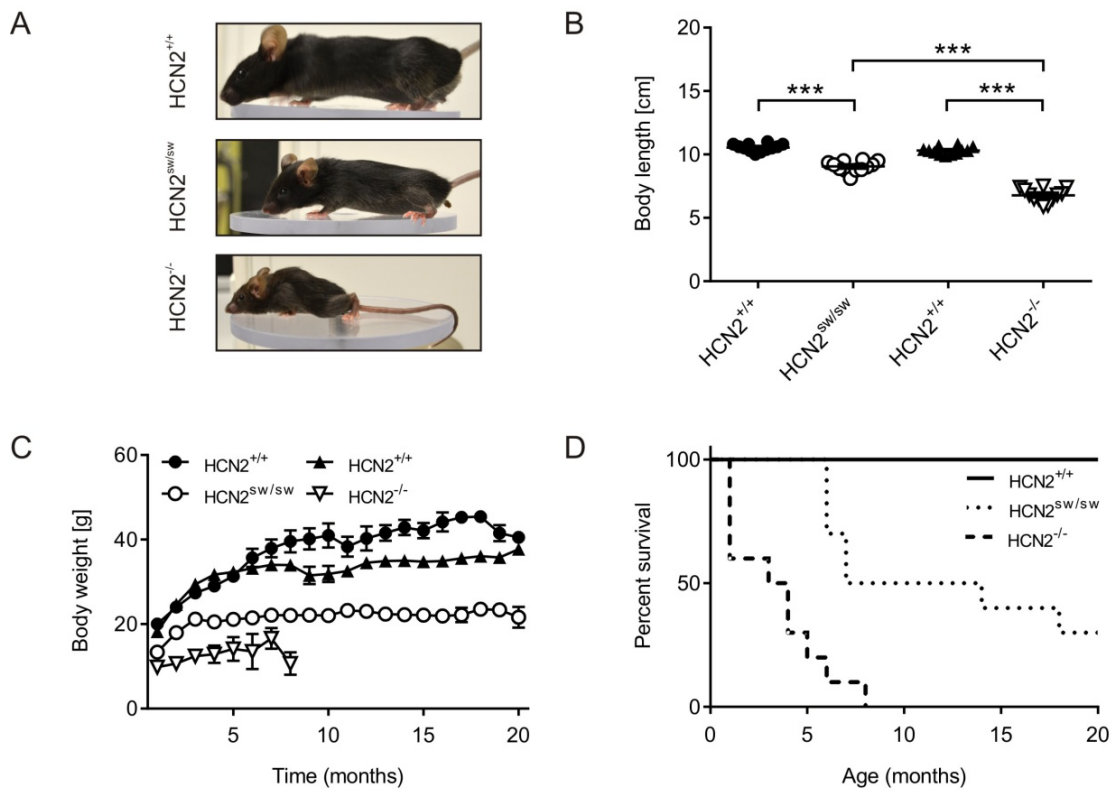


Figure 16: Reduced body growth and shortened lifespan of HCN2^{sw/sw} mice. (A) Pictures taken from HCN2^{+/+}, HCN2^{sw/sw} and HCN2^{-/-} mice (8-week old) to exhibit their differences in appearance. (B) Body length assessment of HCN2^{sw/sw} (○), HCN2^{-/-} (▼) and their own WT controls (8-week old) (●: littermates of HCN2^{sw/sw} mice, ▲: littermates of HCN2^{-/-} mice). No significant effect of background was observed $F=1.569$, $p=0.1545$ ($n=12$). (C) Body weights of HCN2^{sw/sw} (○), HCN2^{-/-} (▼) and their own WT littermates (●: littermates of HCN2^{sw/sw} mice, ▲: littermates of HCN2^{-/-} mice) were plotted as a function of age ($n=10$). (D) Survival rates of HCN2^{sw/sw} (dotted line), HCN2^{-/-} (dashed line) and their own control mice (solid line) ($n=10$). Data were presented as mean \pm SEM. *** $p<0.001$ (B, Bonferroni test preceded by two-way ANOVA).

The mean lifespan of HCN2-deficient mice was reduced to 3.4 months while HCN2^{sw/sw} mice had an average lifespan of 12.4 months (Table 8). The maximum lifespan of HCN2^{sw/sw} mice was the same as the background-matched WT mice while that of HCN2-deficient mice was shortened to maximum 8 months (Table 8). These results suggested that the replacement of HCN2 with HCN1 extended the mean and maximum lifespan of HCN2^{sw/sw} mice compared with HCN2-deficient mice. Particularly, the maximal lifespan of HCN2^{sw/sw} mice was extended and a subpopulation is

able to live as long as WT mice. However, there was still a population of HCN2^{sw/sw} mice, which died at the early stage of postnatal development.

Table 8: Mean and maximum lifespan of HCN2^{+/+}, HCN2^{sw/sw} and HCN2^{-/-} mice.

	HCN2 ^{+/+}	HCN2 ^{sw/sw}	HCN2 ^{+/+}	HCN2 ^{-/-}
mean lifespan (months)	20.0 ± 0.0	12.4 ± 2.1	20.0 ± 0.0	3.4 ± 0.8
max. lifespan (months)	20	20	20	8

3.4.2 Ataxic gait in HCN2^{sw/sw} mice

It was reported that HCN2-deficient mice displayed ataxia (Ludwig et al., 2003). To determine the extent of the ataxic gait in HCN2^{sw/sw} mice, footprints of mice (Figure 17A) were analyzed based on measurements of stride length, hindpaw angle forepaw base and hindpaw base.

Both HCN2^{sw/sw} and the HCN2^{-/-} mice showed a reduced stride length compared to the background-matched WT mice (Figure 17B, HCN2^{+/+}(●): 6.1 ± 0.1 cm, HCN2^{sw/sw}: 4.7 ± 0.2 cm, p<0.0001; HCN2^{+/+}(▲): 6.4 ± 0.1 cm, HCN2^{-/-}: 3.5 ± 0.1 cm, p<0.0001). Notably, the reduction in stride length in HCN2^{-/-} mice was greater than that in HCN2^{sw/sw} mice (p<0.0001). This was in accordance with the previously observed results in the body lengths (Chapter 3.4.1).

Abnormal gait pattern is usually associated with an increased hindpaw angle and a wider fore- and hindpaw base in mice. The hindpaw angle is the angle between the two outmost toes of hind paws and the base is the distance between forepaws or hindpaws normalized to body length. The average hindpaw angle of HCN2-deficient mice was 180 degree, which was 13 degree larger than that of their WT controls (Figure 17C, HCN2^{+/+}(▲): 167 ± 2 degree, HCN2^{-/-}: 180 ± 2 degree, p=0.0002). HCN2^{sw/sw} mice also exhibited a larger hindpaw angle than their background-matched WT controls (Figure 17C, HCN2^{+/+}(●): 161 ± 2 degree, HCN2^{sw/sw}: 173 ± 1 degree, p=0.0004). HCN2^{sw/sw} and HCN2^{-/-} mice showed significantly wider forepaw base relative to their own background-matched WT controls (Figure 17D, HCN2^{+/+}(●): 0.15 ± 0.01, HCN2^{sw/sw}: 0.27 ± 0.01, p<0.0001; HCN2^{+/+}(▲): 0.16 ± 0.01, HCN2^{-/-}: 0.22 ± 0.01, p<0.0001).

HCN2^{sw/sw} mice showed a normal hindpaw base (Figure 17E, HCN2^{+/+}(●): 0.24 ± 0.01 , HCN2^{sw/sw}: 0.27 ± 0.01) while HCN2^{-/-} mice exhibited a great increase in hindpaw base compared to their own WT controls (Figure 17E, HCN2^{+/+}(▲): 0.25 ± 0.01 , HCN2^{-/-}: 0.39 ± 0.02 , $p < 0.0001$). Compared to HCN2^{-/-} mice, HCN2^{sw/sw} mice showed narrower forepaw and hindpaw base ($p = 0.0008$ for forepaw base, $p < 0.0001$ for hindpaw base). These results indicated that the replacement of HCN2 by HCN1 attenuated the abnormal gait.

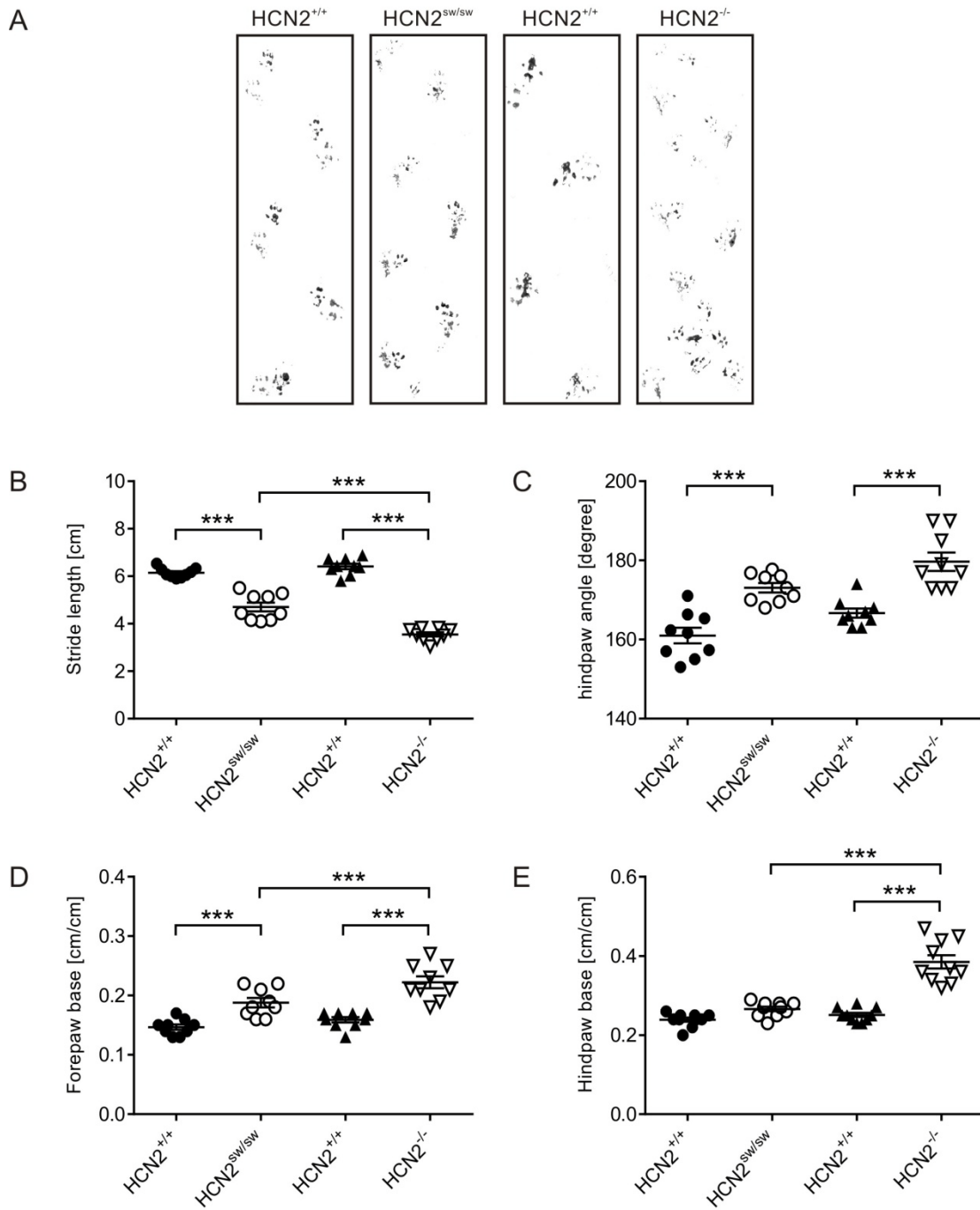


Figure 17: Ataxic gait of HCN2^{sw/sw} mice in footprint analysis. (A) Representative footprints of HCN2^{sw/sw}, HCN2^{-/-} and WT control mice. Forepaws in darker color and hindpaws in grey color. Differences in stride length (B), hindpaw angle (C), forepaw base (D) and hindpaw base (E) among WT (●: littermates of HCN2^{sw/sw} mice, ▲: littermates of HCN2^{-/-} mice), HCN2^{sw/sw} (○) and HCN2^{-/-} (▼) mice (8-week old) were analyzed. Data were presented as mean ± SEM. n=12. *** p < 0.001 (B-E, Bonferroni test preceded by two-way ANOVA).

3.4.3 Motor deficit in HCN2^{sw/sw} mice

An abnormal gait in mice consequently leads to reduced locomotor activity, e.g. HCN2-null mice showed hypoactivity and motor dysfunction (Ludwig et al., 2003). To determine whether HCN2^{sw/sw} mice display motor deficits, an open field test was performed followed by the measurement of velocity, distance travelled and locomotion time.

The representative movement traces of all genotypes were shown in Figure 18A. Thigmotaxis, the tendency to move close to the walls, was observed in all animals. It is a natural response of mice when they are confronted to unfamiliar environments. In contrast to the background-matched WT mice, HCN2^{sw/sw} mice explored the center of the open-field arena less often and HCN2^{-/-} mice almost leaned on the walls. Although the extent of thigmotaxis is used as an index of anxiety under normal circumstance, we speculate the thigmotaxis in HCN2^{sw/sw} and HCN2^{-/-} mice was attributed to severe motor dysfunction.

Compared to their WT littermates, HCN2^{-/-} mice also had reduced velocity (Figure 18B, HCN2^{+/+}(▲): 18.34 ± 0.41 cm/s, HCN2^{-/-}: 11.86 ± 0.13 cm/s, p<0.0001), shortened travel distance (Figure 18C, HCN2^{+/+}(▲): 15.8 ± 1.1 m, HCN2^{-/-}: 3.44 ± 0.7 m, p<0.0001) and less locomotion time (Figure 18D, HCN2^{+/+}(▲): 28.6% ± 1.5, HCN2^{-/-}: 9.5% ± 1.7, p<0.0001). This observation is in accordance with that of Ludwig et al. (2003). HCN2^{sw/sw} mice exhibited also lower velocity (Figure 18B, HCN2^{+/+}(●): 20.1 ± 0.4 cm/s, HCN2^{sw/sw}: 13.22 ± 0.4 cm/s, p<0.0001), shorter distance moved (Figure 18C, HCN2^{+/+}(●): 19.4 ± 1.9 m, HCN2^{sw/sw}: 7.9 ± 1.6 m, p<0.0001) and less locomotion time (Figure 18D, HCN2^{+/+}(●): 31.4% ± 2.6, HCN2^{sw/sw}: 18.9% ± 3.2, p<0.0001) than the background-matched WT mice. Only a slight increase in the locomotion time (p=0.032) was observed in HCN2^{sw/sw} mice when compared with HCN2^{-/-} mice. These results suggested motor deficits in HCN2^{sw/sw} mice.

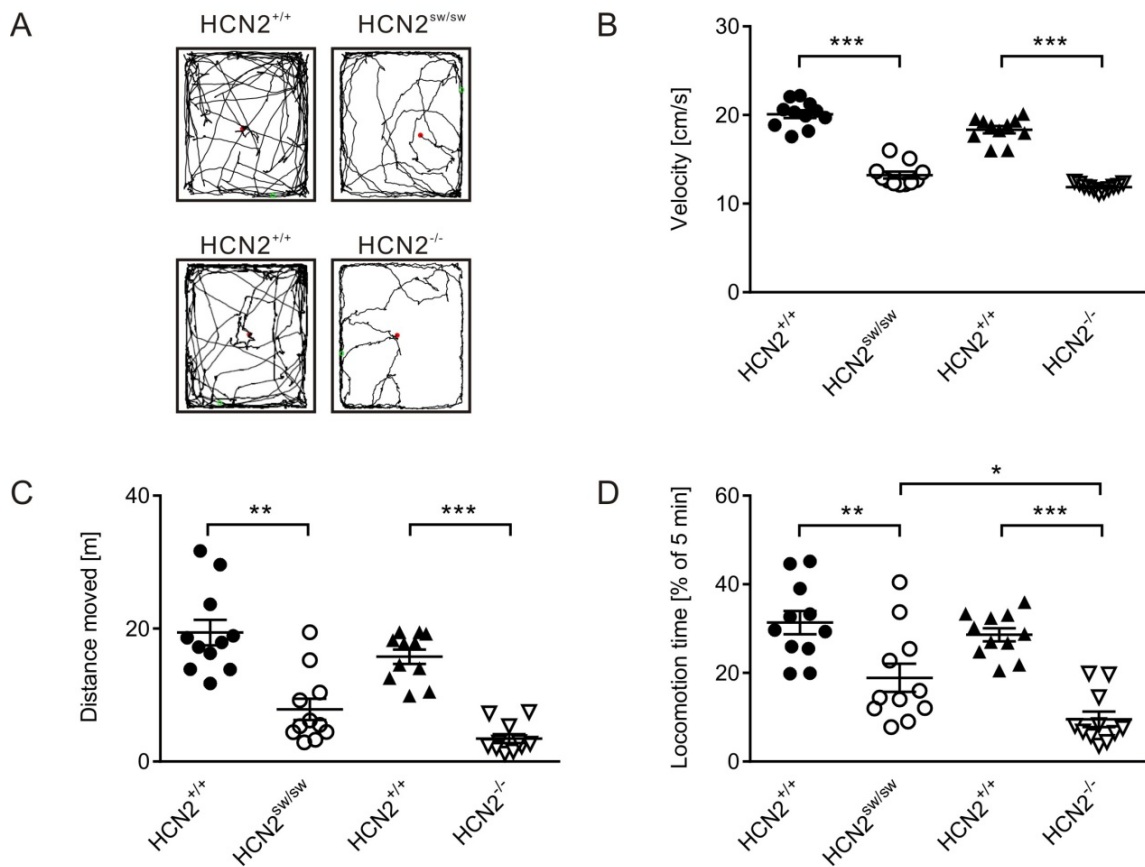


Figure 18: Motor deficits of HCN2^{sw/sw} mice in open field test. (A) Representative traces of movement of HCN2^{sw/sw}, HCN2^{-/-} and WT controls. The red dots indicated the release points. (B-D) Comparison of locomotion speed, distance moved and locomotion time among HCN2^{sw/sw} (○), HCN2^{-/-} (▼) and their own WT controls (●: littermates of HCN2^{sw/sw} mice, ▲: littermates of HCN2^{-/-} mice). No significant effect of background were observed (velocity: $F=1.061$, $p=0.4207$; distance: $F=0.7761$, $p=0.6505$; locomotion time: $F=0.8590$, $p=0.5792$). All mice were around 8-week old. Data were presented as mean \pm SEM. $n=12$. * $p<0.05$, ** $p<0.01$, *** $p<0.001$ (B-D, Bonferroni test preceded by two-way ANOVA).

3.4.4 Impaired visual discrimination capacity in HCN2^{sw/sw} mice

In the thalamus, HCN2 is abundantly expressed. Ablation of HCN2 channels result in a great reduction in I_h (~80%) in the TC neurons, which in turn promotes the burst firing activity (Ludwig et al., 2003). Particularly, the spindle wave activity is considered to be crucial for memory consolidation, sensorimotor coordination and learning (Khazipov et al., 2004; Fogel and Smith, 2011). To determine whether FLAG-HCN1 in the thalamus of HCN2^{sw/sw} mice could help to

regulate thalamic activities, a two-alternative forced-choice visual discrimination task was performed as described by Trevino et al. (2013). Although $HCN2^{-/-}$ mice are not capable to swim due to the gravely impaired motor function, adult $HCN2^{sw/sw}$ mice are capable to swim in a correct swimming posture.

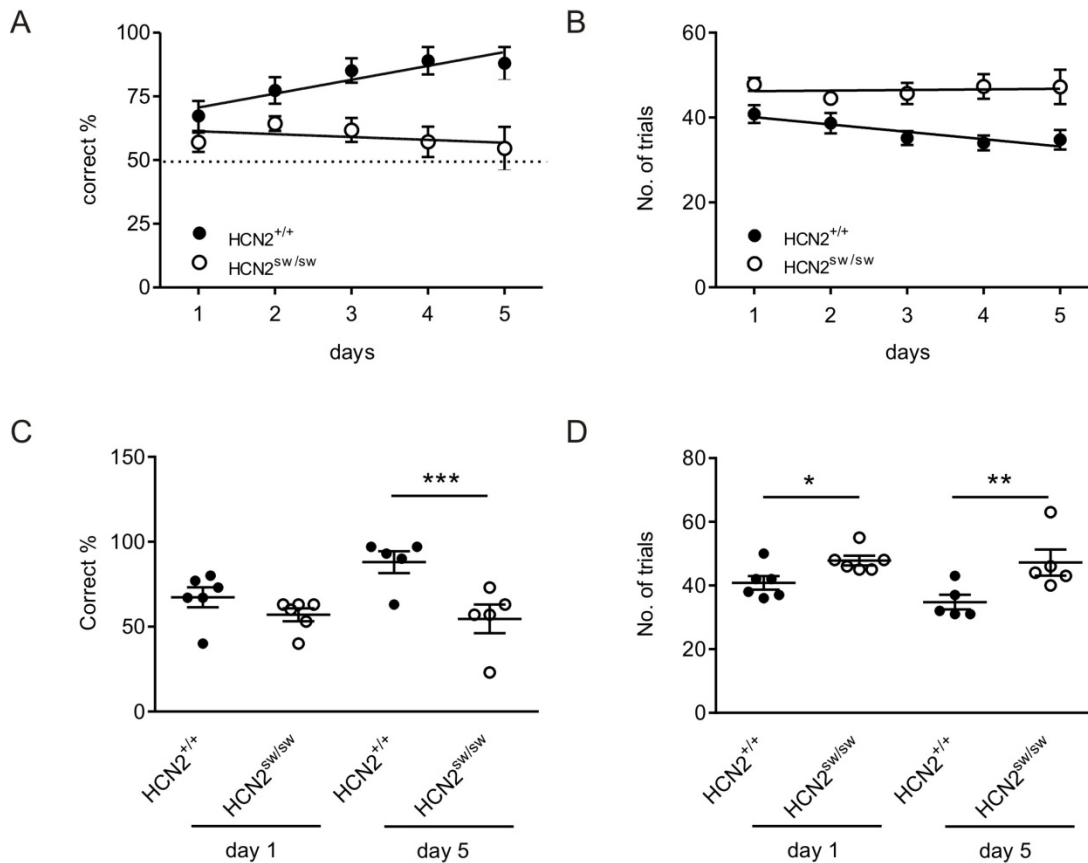


Figure 19: Visual discrimination deficits of $HCN2^{sw/sw}$ mice in a modified visual discrimination task. (A) The probability to find the hidden platform in the first trial of a training unit was plotted as a function of training days. Random choice behavior depicted by the dotted line at 50%. Learning was reflected by the slope of the linear regression best-fit line. (B) The number of trials per day was plotted as a function of training days. (C) Comparison of correct% on the first and last training day. (D) Comparison of the number of trials on the first and last day. ●: $HCN2^{+/+}$, ○: $HCN2^{sw/sw}$. All mice were around 8-week old. Data were presented as mean \pm SEM. n=6. (A-B) Linear regression analysis. (C-D) * $p < 0.05$, ** $p < 0.01$, *** $p < 0.001$, student's t test followed by Mann-Whitney u test.

A successful discrimination in WT mice was characterized by the increasing probability of making a correct choice in the first presentation of a training unit (correct%) (Figure 19A, HCN2^{+/+}, slope of regression line: 5.447 ± 1.727 , $p=0.0039$) and the decreasing number of trials per day (Figure 20B, HCN2^{+/+}, slope of regression line: -1.727 ± 0.645 , $p=0.0124$), while HCN2^{sw/sw} did not show any learning (Figure 19A, HCN2^{sw/sw}, slope of regression line: -1.123 ± 1.648 , $p=0.5015$; Figure 20B, HCN2^{sw/sw}, slope of regression line: 0.1426 ± 0.795 , $p=0.8591$). On the first training day, WT and HCN2^{sw/sw} had similar probability to make a correct choice (Figure 19C, day 1: $67.33\% \pm 5.87$ for HCN2^{+/+}, $57.00\% \pm 3.75$ for HCN2^{sw/sw}, $p=0.1687$), but the number of swimming trials of HCN2^{sw/sw} mice was higher than that of WT mice (Figure 19D, day 1: $40.83\% \pm 2.10$ for HCN2^{+/+}, $47.83\% \pm 1.54$ for HCN2^{sw/sw}, $p=0.0303$), suggesting the born motor deficits in HCN2^{sw/sw} may affect their swimming performance. On the last training day, both parameters were significantly different between WT and HCN2^{sw/sw} mice (Figure 19C, day 5: $88.00\% \pm 6.39$ for HCN2^{+/+}, $54.60\% \pm 8.42$ for HCN2^{sw/sw}, $p=0.0238$; Figure 19D, day 5: $40.83\% \pm 2.10$ for HCN2^{+/+}, $47.83\% \pm 1.54$ for HCN2^{sw/sw}, $p=0.0303$), implicating that HCN2^{sw/sw} mice had poor learning and impaired visual discrimination capacity.

In addition to learning, visual function can also affect the visual discrimination capacity, because the thalamus functions as a relay station in the visual pathway. Optical coherence tomography (OCT) was performed after visual discrimination task to study retinal degeneration (Figure 20A). The normal retinal thickness of HCN2^{sw/sw} mice indicated a regular retinal development in the HCN2^{sw/sw} mice (Figure 20B).

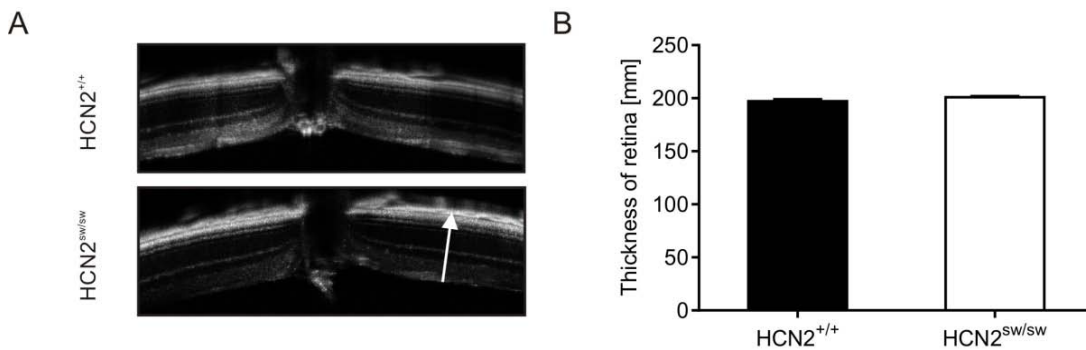


Figure 20: Optical coherence tomography of $HCN2^{+/+}$ and $HCN2^{sw/sw}$ mice. (A) Representative images of retina from $HCN2^{sw/sw}$ and WT mice. (B) Retinal thickness (measured as indicated by the white arrow in A) in WT (black bar) and $HCN2^{sw/sw}$ (open bar) mice. Data were presented as mean \pm SEM. $n = 4$. (B, non-parametric student's t test followed by a Mann-Whitney u test).

3.5 Spike-and-wave discharges in $HCN2^{sw/sw}$ mice

$HCN2^{-/-}$ mice displayed absence epilepsy characterized by synchronized bilateral SWDs in EEG measurement (Ludwig et al., 2003). To determine whether replacing HCN2 with HCN1 could rescue the $HCN2^{sw/sw}$ mice from absence epilepsy, a cortical EEG measurement was performed to detect the SWDs in $HCN2^{sw/sw}$ mice. For EEG measurement, mice were transplanted with an EEG transmitter system from DSI (F20-EET, Data Science International, USA), which can record EEG traces and an electromyogram (EMG) simultaneously.

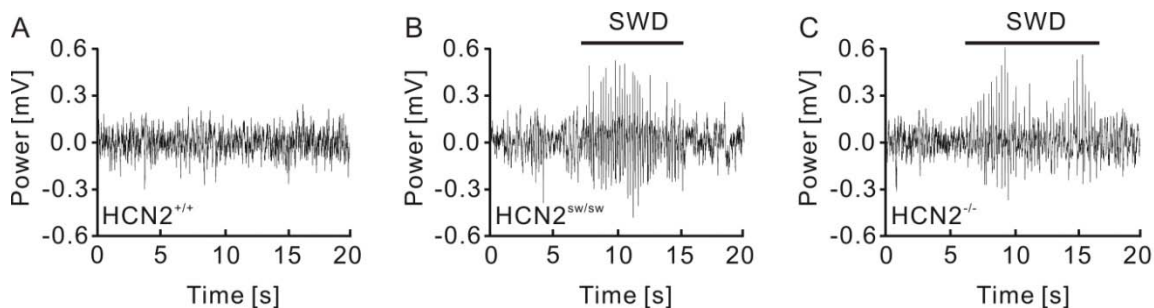


Figure 21: The occurrence of SWD in $HCN2^{sw/sw}$ mice. Characteristic EEG traces of WT (A), $HCN2^{sw/sw}$ (B) and $HCN2^{-/-}$ (C) mice of a 20-second interval. SWDs were indicated in $HCN2^{sw/sw}$ and $HCN2^{-/-}$ mice as a black bar.

SWDs are a hallmark for absence epilepsy that was published previously for the HCN2-null mice (Figure 21C) (Ludwig et al., 2003), whereas healthy WT animals never show SWDs (Figure 21A).

HCN2^{sw/sw} mice also suffered from SWDs (Figure 21B). This indicated that the presence of HCN2 subunits seemed to be essential for a healthy brain function, which cannot be replaced by the HCN1 subunits. The mean length of an SWD did not differ from HCN2^{sw/sw} to HCN2-deficient mice (data not shown).

4. Discussion

Knock-in mice that express an *HCN1* transgene under the control of the HCN2 promoter display ataxia, impaired visual discrimination and absence seizures. The reduced size, shortened lifespan, impaired locomotor activity and epilepsy of the homozygous HCN2-1 switch mice resemble the phenotypes of HCN2^{-/-} animals (Ludwig et al., 2003). Quantitatively, these deficits are less severe. HCN2-deficient mice show a global deletion of HCN2 channels in the CNS without any alterations in other three HCN channels. In contrast, HCN2^{sw/sw} mice express FLAG-HCN1 instead of HCN2, in addition to an unaltered expression level of HCN3 and HCN4. In some brain regions and neurons, such as the thalamus and the dopaminergic neurons of SNc, the distribution pattern of FLAG-HCN1 is in line with that of HCN2 channels. These observations suggest that the abnormality in both genotypes results from the loss of HCN2; however, HCN1 channels can partially substitute HCN2 channels through developing a compensatory mechanism.

This finding expands our current understanding of the relationship between the HCN channel dysfunction and neuronal diseases, such as ataxia and epilepsy. I_h is critical for the rhythmic activity in the thalamus and the regulation of oscillations within the thalamocortical network. In HCN2-deficient mice, deletion of HCN2 reduces I_h by about 80% in the TC neurons, resulting in hyperpolarization of the resting membrane potential, an altered response to excitatory inputs and increasing susceptibility of seizures (Ludwig et al., 2003). Here, we found in EEG measurement that SWDs occurred in HCN2^{sw/sw} mice, suggesting that they also displayed absence epilepsy although HCN2 was replaced by HCN1. Basically, the new FLAG-HCN1 channels are activated in response to hyperpolarization, which could prevent a profound hyperpolarizing shift of resting membrane potential. The proportion of T-type calcium channels present in the inactivated state in the SW TC neurons would be higher than in HCN2-deficient cells where more T-type calcium channels are in the closed state. This minor alteration in HCN2^{sw/sw} mice would contribute little to normalizing the resting membrane potential, so the T-type calcium channels are still easier to be activated by excitatory inputs. Thus, TC neurons in HCN2^{sw/sw} mice have a higher seizure propensity than that in WT mice. In addition to hyperpolarized resting membrane potential, the responsiveness of I_h to cAMP is also greatly reduced, because the new HCN1 channels are only weakly regulated by cAMP. However, the cAMP modulation of HCN channels

plays a key role in the transition between the burst and the tonic firing mode of TC neurons. Loss of modulation by cAMP, the SW TC neurons would show sustained burst firing and higher seizure susceptibility. The cAMP-insensitivity of FLAG-HCN1 channels would also affect the spindle wave activity. Physiologically, a delayed upregulation of I_h is caused by the Ca^{2+} -triggered cAMP synthesis and contributes to termination of the spindle wave activity through diminishing the prolonged low-threshold Ca^{2+} spikes (Biel et al., 2009). In the case that HCN1 is less responsive to cAMP, I_h would not be sufficiently upregulated by the intracellular cAMP, therefore the termination of the spindle wave would be prolonged.

Taken together, the key role of HCN2 in thalamic rhythmogenesis might result from its specific biophysical properties. Speculatively, the biophysical properties of I_h in the SW TC neurons would be altered regarding the following three aspects. 1) Voltage dependence. In WT TC neurons, the $V_{0.5}$ value of I_h is -88 mV, whereas it shifts to -115 mV in the HCN2-null TC neurons. Given the existence of homomeric HCN1 channels or heteromeric HCN1/4 channels in the SW TC neurons, the $V_{0.5}$ of I_h in these cells would be intermediate between that in WT and HCN2-null cells. 2) Current density. The I_h density in HCN2-deficient TC neurons is nearly absent due to lack of the I_h -conducting channels. The FLAG-HCN1 channels in SW TC neurons to some extent preserve the I_h conductance, so the I_h density would be higher compared to HCN2-deficient TC neurons. Whether the I_h density in SW TC neurons is comparable to that in WT cells is hard to be estimated. The first reason is that the single-channel conductance of HCN1 and HCN2 are different. Available data for the single-channel properties of HCN channels are controversial because they are ranged from 0.68 to 9.7 pS when measured in heterologous expression system or in native cortical and hippocampal pyramidal cells (Johnson and Zagotta, 2005; Dekker and Yellen, 2006; Kole et al., 2006; Thon et al., 2013). Michels et al. (2005) have reported that HCN2 had significantly larger single-channel conductance than HCN1 when expressed in CHO cells (HCN1: 12.91 ± 0.92 pS, HCN2: 34.63 ± 2.43 pS). Consistently Brandt et al. (2009) have demonstrated almost identical values (HCN1: 13.30 ± 1.00 pS, HCN2: 34.63 ± 2.43 pS), however it still lacks data of the single-channel properties of native I_h in the thalamus. The second reason is that the channel density of the new HCN1 probably differs from that of the native HCN2 in TC neurons. Quantitative PCR analyses revealed that the quantity of FLAG-HCN1 mRNA in HCN2^{sw/sw} mice was likely fewer than that of HCN2 mRNA in WT mice (Table 2), suggesting a less transcription of FLAG-HCN1 mRNA. Due to lack of quantification at protein level, a final conclusion that the

number of HCN channels in SW TC neurons is fewer than that in WT cells cannot be drawn. 3) Response to cAMP binding. The property of I_h in the hippocampal CA1 pyramidal neurons resembles that mediated by the homomeric HCN1 channels in a heterologous expression system, showing weak responsiveness to intracellular cAMP injection (Santoro et al., 2000). Likewise, replacing HCN2 by HCN1 in the thalamus would also reduce the sensitivity of thalamic I_h to cAMP. To support these hypotheses, the properties of I_h and the resting membrane potential of SW TC neurons should be determined.

In addition to the alterations in HCN channels themselves, the neuronal networks where HCN channels are embedded in may affect the properties of I_h via channel interactors. Due to the tight linkage between epileptogenesis and thalamocortical circuit function, neuroregulators that may regulate the intrinsic rhythmic activity of the thalamocortical loop by gating HCN channels are of great interests. Nitric oxide (NO), a diffusible messenger, has been found to decline the oscillatory activity by shifting the voltage-dependence of I_h in TC neurons to more depolarizing potential (about 7 mV) and promoting the inactivation of I_{CaT} (Pape and Mager, 1992; Yang and Cox, 2007, 2008). Recently, Kopp-Scheinflug et al. (2015) unraveled that NO selectively enhanced the HCN2-mediated I_h in a cGMP-dependent manner, while suppressed the HCN1-mediated I_h independent to cGMP. Given an unaltered NO production in the cholinergic terminals originated from the brainstem nuclei in HCN2^{sw/sw} mice, the newly generated HCN1 channels is supposed to be suppressed by NO, which shifts the half-activation of I_h in TC neurons to more hyperpolarizing potential, removes the inactivation of T-type calcium channels and promotes burst firing activity. Similar to the unresponsiveness to cAMP, HCN1 channels are also less sensitive to cGMP. This insensitivity makes the SW TC neurons hard to achieve the transition from the burst to tonic firing activity. KCNE2, also named Mink-related protein1, is an auxiliary subunit of HCN channels. It has been reported that targeted deletion of KCNE2 impairs HCN channel function in thalamocortical circuit (Ying et al., 2012). In heterologous expressing system with whole cell recording at -120 mV, the current density of HCN1-mediated I_h increased from 45.6 to 68.7pA/pF while that of HCN2-mediated I_h increased from 41.8 to 86.6pA/pF in the presence of KCNE2. The half-activation potentials of both HCN channels were not affected by KCNE2. At single-channel level, KCNE2 significantly reduced the availability of HCN1 rather than HCN2, but increased P_o , prolonged the mean open time and decreased the mean closed time of HCN2 rather than HCN1 (Brandt et al., 2009). Given a normal expression of KCNE2 in the

thalamus of HCN2^{sw/sw} mice, the current density of I_h may be less upregulated by KCNE2, resulting in an increased membrane excitability in TC neurons.

In brain networks, the thalamocortical circuit cannot be seen isolated; its oscillatory activity is in fact regulated by excitatory or inhibitory inputs from other brain structures involved in a variety of neuronal pathways. Basal ganglia comprising of multiple brain structures, such as the striatum, the subthalamic nuclei (STN), the SN and the GP (Figure 22) functionally connect the cortex and thalamus. HCN channels are widely expressed in the basal ganglia and play important roles in regulation of neuronal excitability and rhythmic activity (Chu and Zhen, 2010; Chan et al., 2011; Deng et al., 2015). Basal ganglia are primarily known to control motor functions so that voluntary actions can be smoothly executed. There are three pathways involved in motor controlling: 1) In the direct pathway, striatum receives glutamatergic inputs from cortex and inhibits substantia nigra pars reticular/internal segment of globus pallidus (SNr/GPi), which are GABAergic and originally inhibit thalamic neurons (Figure 22B) (Yasoshima et al., 2005). 2) In the indirect pathway, STN activates SNr/GPi neurons, which originally send inhibitory input to thalamus, so that the motor activity signal transferring to cortex will be broken (Figure 22A). Previous study demonstrated the synchronous, burst firing of STN and GPe neurons in the PD mouse models (Kase et al., 2012). Further, Deng et al. (2015) revealed that HCN channels bidirectionally modulated the activity of the STN *in vivo*, owing to the heteromerization of HCN subunits. The proportion of cAMP-insensitive HCN1 subunits would increase in the STN of HCN2^{sw/sw} mice, I_h activity in the SW STN neurons would be reduced due to diminished cAMP response. As a consequence, the membrane excitability of STN neurons would be increased and the occurrence of SWDs would also be elevated. The burst firing of GPe neurons will inhibit STN neurons, so that the inhibition of SNr/GPi on the thalamus would be removed and the motor activity can be further passed on the cortex, causing resting tremors in Parkinson's disease. The altered firing activity (increased average firing rate and tend to fire in burst) is attributed to a decrease in I_h and the dopamine deficiency (Levy et al., 2002). In other primate and rat parkinsonian models, it has been found that GPi/SNr was also involved in motor dysfunctions regarding their enhanced firing activities (Bergman et al., 1994; Abedi et al., 2013). The STN has been shown to strongly express HCN2, suggesting that HCN2-mediated I_h is likely to be a key factor in regulation the intrinsic activity of these neurons. We hypothesize that I_h in the basal ganglia of HCN2-deficient mice would be greatly reduced; the resulting increase in firing activity

would promote burst firing. This dysregulation of I_h would affect the regulation of dopaminergic pathways, thus $HCN2^{-/-}$ mice show parkinsonian tremors. On the other hand, the FLAG-HCN1 in the basal ganglia of $HCN2^{sw/sw}$ mice would attenuate the reduction in I_h , to some extent preserve the function of dopaminergic neurons and thereby partially restore the motor function in $HCN2^{sw/sw}$ mice. 3) In the nigrostriatal pathway (Figure 22), the death of dopaminergic neurons in SNc results in an insufficient release of dopamine (DA) into synaptic cleft in striatum. Lacking dopamine projection, motor symptoms are present in patients with Parkinson's disease (PD). The whole-body tremor, one of the motor symptoms of PD, and the general motor dysfunction are observed in $HCN2^{sw/sw}$ and $HCN2$ -null mice with less severity in $HCN2^{sw/sw}$. The pathological behaviors are supposed to be associated with a changed oscillatory activity in SNc DA neurons, which is regulated by HCN2-mediated I_h (Franz et al., 2000; Neuhoff et al., 2002; Xue et al., 2012).

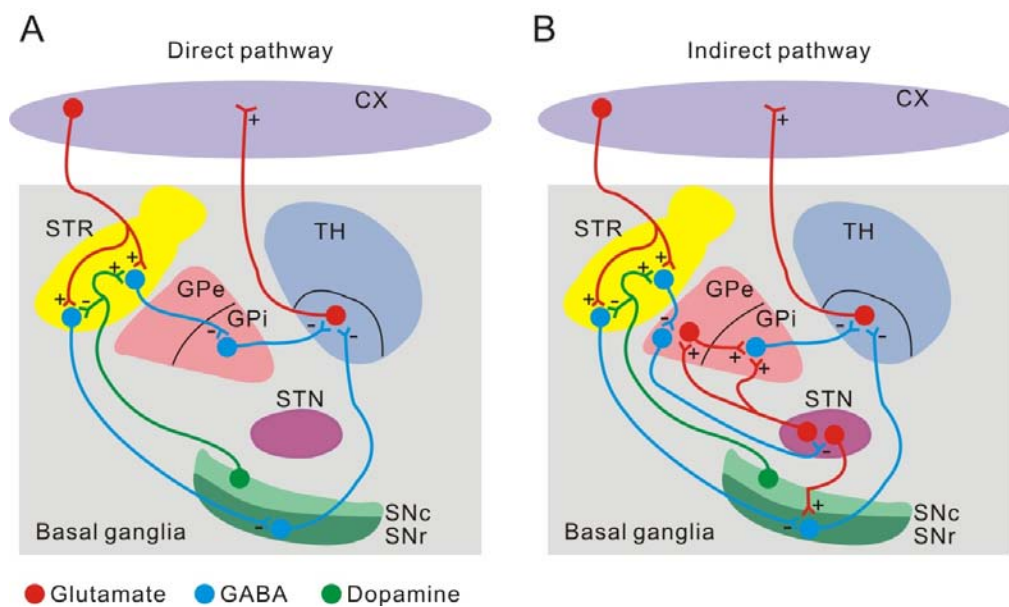


Figure 22: Schematic diagram of the basal ganglia circuits. The striatum is the primary input station in basal ganglia and receives excitatory input from the cortex. From Striatum the two pathways diverge: (A) The direct pathway sends inhibitory inputs directly to SNr and GPi. (B) The indirect pathway first projects to GPe and STN, then back to SNr and GPi. The SNr and GPi are the main output nuclei in basal ganglia. They normally send inhibitory connections to the thalamus, which projects to the cortex. Thus the basal ganglia loop is completed. The nigrostriatal pathway (green) transmits dopamine from SNc to the striatum. TH: thalamus, STR: striatum, Cx: cortex, GPe: external segment of globus pallidus, GPi: internal segment of globus pallidus, SNc: substantia nigra pars compacta, SNr: substantia nigra pars reticular, STN: subthalamic nuclei. Adapted from [1].

In addition to motor deficits, impaired visual discrimination capacity has been observed in freely moving HCN2^{sw/sw} mice. The performance of mice in the visual discrimination task is determined by two factors: one is the visual discrimination capacity, which is determined by the visual function in retina and the visual processing involving the dorsal lateral geniculate nuclei (dLGN) and primary visual cortex. Although no degeneration was observed in the retina of HCN2^{sw/sw} mice, it is still necessary to perform electroretinogram (ERG) to ensure a normal visual function. Recently, it has been revealed that nitric oxide (NO) can amplify the neuronal activity on dLGN in a cGMP-dependent manner, suggesting the HCN2-mediated I_h might be upregulated by cGMP (Lima et al., 2014). In HCN2^{sw/sw} mice, the FLAG-HCN1 would be weakly modulated by cGMP. The resulting reduction in I_h would impair the amplification of visual signals from retina in the thalamus. As a consequence, the visual detection in the primary visual cortex would be affected. The other one is the learning efficiency. Visual discrimination in mice can only be studied by learning, and learning can in turn promote visual discrimination. Although visual perceptual learning consolidated in sleep and the consolidation is associated with spindle activities (Bang et al., 2014), the severe motor deficits are still considered to be the main reason for learning deficits.

In conclusion, the study demonstrates a partial compensatory mechanism developed in HCN2^{sw/sw} mice by replacing HCN2 with HCN1. This substitution substantially attenuates the severe ataxic phenotypes and motor deficits but cannot suppress SWDs and the genesis of absence epilepsy. HCN1 and HCN2 are coexpressed in many neurons and form functional heteromer to increase the diversity of local I_h . However, due to their distinct biophysical properties (activation and deactivation kinetics and the extent of regulation by cAMP), the HCN2-encoded component of neuronal I_h could not be recapitulated by the substitution, particularly in the neurons where HCN2 predominates. This finding supports the idea that the role of HCN2 in the generation and regulation of thalamic rhythmic activity is critical and demonstrates the important contribution of the cAMP-mediated acceleration on channel activation to the regulation of neuronal network activity.

5. Summary

Hyperpolarization-activated cyclic nucleotides-gated channels (HCN) play a critical role in the regulation of neuronal rhythmic activity. HCN1 and HCN2 differ in the voltage-dependence of channel activation and the responsiveness to cAMP, the relevance of such differences to the neuronal function remains unclear. To get a better understanding of the individual contribution of the channel properties to the regulation of rhythmic activity in neuronal networks, a novel HCN2 replacement mouse model (HCN2-1 switch mice) was analyzed, in which the cAMP-sensitive HCN2 is replaced by HCN1 that is weakly modulated by cAMP.

Biochemical characterization confirmed the expression of FLAG-HCN1 instead of HCN2 at both mRNA and protein levels without altering the expression of HCN3 and HCN4 mRNA. The expression pattern of FLAG-HCN1 channels in the hippocampus, cerebellum, thalamus and substantia nigra was similar to that of native HCN2 channels. The brain morphology of HCN2-1 switch mice was normal. Moreover, HCN2-1 switch mice displayed attenuated ataxia and motor dysfunctions as compared to HCN2-deficient mice, suggesting that a partial compensatory mechanism involving various neuronal circuits in the brain networks was developed. Notably, HCN2-1 switch mice showed impaired visual discrimination capacity and displayed absence epilepsy characterized by the bilateral synchronized SWDs in EEG measurement. It demonstrates the irreplaceable role of thalamic HCN2 channels in the maintenance of a normal visual processing, the regulation of rhythmic activity of TC neurons and the generation of normal oscillatory activity in the thalamocortical circuit.

Zusammenfassung

HCN Kanäle spielen eine entscheidende Rolle in der Regulation neuronaler rhythmischer Aktivität. HCN1 und HCN2 unterscheiden sich in der Spannungsabhängigkeit ihrer Kanalaktivierung und der Modulationsfähigkeit durch cAMP, die Auswirkungen dieser Unterschiede auf neuronale Funktionen sind ungeklärt. Um ein besseres Verständnis für den individuellen Beitrag der Kanaleigenschaften zur Regulation der rhythmischen Aktivität in neuronalen Netzwerken zu erhalten, wurde ein neues Mausmodell (HCN2-1 switch Mäuse) analysiert, in dem das cAMP-sensitive HCN2-Gen durch das HCN1-Gen ersetzt wurde, welches nur schwach durch cAMP moduliert werden kann.

Biochemische Charakterisierungen bestätigten die Expression von FLAG-HCN1 aus dem HCN2 Locus sowohl auf mRNA- als auch auf Proteinebene. Die Expression von HCN3 und HCN4 mRNA wurde nicht beeinträchtigt. In manchen Gehirngebieten und Neuronen, z.B. im Thalamus und in den dopaminergen Neuronen in der Substantia Nigra weist der neu generierte FLAG-HCN1 ähnliche regionale Verteilungsmuster auf wie der native HCN2. HCN2-1 switch Mäuse zeigten normale Hirnmorphologie. Darüber hinaus zeigten sie eine schwächere Ataxie und Bewegungsstörungen im Vergleich zu HCN2-defizienten Mäusen, was einen Teilkompensationsmechanismus in HCN2 switch Mäusen vermuten lässt. Desweiteren könnte dieser Kompensationsmechanismus an einer Vielzahl von Schaltkreisen im Gehirn beteiligt sein. Bemerkenswert ist, dass HCN2-1 switch Mäuse eine Beeinträchtigung in der visuellen Unterscheidungsfähigkeit zeigten und Absenceepilepsie wie HCN2-defiziente Mäuse entwickelten, welche durch bilaterale synchronisierte Spike-Wave-Entladungen in EEG-Messungen gekennzeichnet ist. Dies demonstriert die nicht ersetzbare Rolle von thalamischem HCN2 bei der Aufrechterhaltung einer normalen visuellen Verarbeitung, der Regulation der rhythmischen Aktivität von TC Neuronen und der Erzeugung von normaler Oszillationsaktivität des thalamocorticalen Schaltkreises.

6. Literatures

- Abbas SY, Ying SW, Goldstein PA (2006) Compartmental distribution of hyperpolarization-activated cyclic-nucleotide-gated channel 2 and hyperpolarization-activated cyclic-nucleotide-gated channel 4 in thalamic reticular and thalamocortical relay neurons. *Neuroscience* 141:1811-1825.
- Abedi PM, Delaville C, De Deurwaerdere P, Benjelloun W, Benazzouz A (2013) Intrapallidal administration of 6-hydroxydopamine mimics in large part the electrophysiological and behavioral consequences of major dopamine depletion in the rat. *Neuroscience* 236:289-297.
- Akimoto M, Zhang Z, Boulton S, Selvaratnam R, VanSchouwen B, Gloyd M, Accili EA, Lange OF, Melacini G (2014) A mechanism for the auto-inhibition of hyperpolarization-activated cyclic nucleotide-gated (HCN) channel opening and its relief by cAMP. *The Journal of biological chemistry* 289:22205-22220.
- Atkinson SE, Williams SR (2009) Postnatal development of dendritic synaptic integration in rat neocortical pyramidal neurons. *Journal of neurophysiology* 102:735-751.
- Bang JW, Khalilzadeh O, Hamalainen M, Watanabe T, Sasaki Y (2014) Location specific sleep spindle activity in the early visual areas and perceptual learning. *Vision research* 99:162-171.
- Bergman H, Wichmann T, Karmon B, DeLong MR (1994) The primate subthalamic nucleus. II. Neuronal activity in the MPTP model of parkinsonism. *Journal of neurophysiology* 72:507-520.
- Biel M, Wahl-Schott C, Michalakis S, Zong X (2009) Hyperpolarization-activated cation channels: from genes to function. *Physiological reviews* 89:847-885.
- Bittner KC, Andrasfalvy BK, Magee JC (2012) Ion channel gradients in the apical tuft region of CA1 pyramidal neurons. *PloS one* 7:e46652.
- Brager DH, Lewis AS, Chetkovich DM, Johnston D (2013) Short- and long-term plasticity in CA1 neurons from mice lacking h-channel auxiliary subunit TRIP8b. *Journal of neurophysiology* 110:2350-2357.
- Brandt MC, Endres-Becker J, Zagidullin N, Motloch LJ, Er F, Rottlaender D, Michels G, Herzig S, Hoppe UC (2009) Effects of KCNE2 on HCN isoforms: distinct modulation of membrane expression and single channel properties. *American journal of physiology Heart and circulatory physiology* 297:H355-363.
- Budde T, Caputi L, Kanyshkova T, Staak R, Abrahamczik C, Munsch T, Pape HC (2005) Impaired regulation of thalamic pacemaker channels through an imbalance of subunit expression in absence epilepsy. *The Journal of neuroscience : the official journal of the Society for Neuroscience* 25:9871-9882.
- Cao-Ehlker X, Zong X, Hammelmann V, Gruner C, Fenske S, Michalakis S, Wahl-Schott C, Biel M (2013) Up-regulation of hyperpolarization-activated cyclic nucleotide-gated channel 3 (HCN3) by specific interaction with K⁺ channel tetramerization domain-containing protein 3 (KCTD3). *The Journal of biological chemistry* 288:7580-7589.
- Chan CS, Glajch KE, Gertler TS, Guzman JN, Mercer JN, Lewis AS, Goldberg AB, Tkatch T, Shigemoto R, Fleming SM, Chetkovich DM, Osten P, Kita H, Surmeier DJ (2011) HCN channelopathy in external globus pallidus neurons in models of Parkinson's disease. *Nature neuroscience* 14:85-92.

- Chen S, Wang J, Siegelbaum SA (2001) Properties of hyperpolarization-activated pacemaker current defined by coassembly of HCN1 and HCN2 subunits and basal modulation by cyclic nucleotide. *The Journal of general physiology* 117:491-504.
- Chu HY, Zhen X (2010) Hyperpolarization-activated, cyclic nucleotide-gated (HCN) channels in the regulation of midbrain dopamine systems. *Acta pharmacologica Sinica* 31:1036-1043.
- Chung WK, Shin M, Jaramillo TC, Leibel RL, LeDuc CA, Fischer SG, Tzilianos E, Gheith AA, Lewis AS, Chetkovich DM (2009) Absence epilepsy in apathetic, a spontaneous mutant mouse lacking the h channel subunit, HCN2. *Neurobiology of disease* 33:499-508.
- Dekker JP, Yellen G (2006) Cooperative gating between single HCN pacemaker channels. *The Journal of general physiology* 128:561-567.
- Deng WS, Jiang YX, Han XH, Xue Y, Wang H, Sun P, Chen L (2015) HCN Channels Modulate the Activity of the Subthalamic Nucleus In Vivo. *Journal of molecular neuroscience : MN* 55:260-268.
- Destexhe A, Contreras D, Steriade M, Sejnowski TJ, Huguenard JR (1996) In vivo, in vitro, and computational analysis of dendritic calcium currents in thalamic reticular neurons. *The Journal of neuroscience : the official journal of the Society for Neuroscience* 16:169-185.
- DiFrancesco D (1981) A study of the ionic nature of the pace-maker current in calf Purkinje fibres. *The Journal of physiology* 314:377-393.
- DiFrancesco D, Tortora P (1991) Direct activation of cardiac pacemaker channels by intracellular cyclic AMP. *Nature* 351:145-147.
- Fath T, Ke YD, Gunning P, Gotz J, Ittner LM (2009) Primary support cultures of hippocampal and substantia nigra neurons. *Nature protocols* 4:78-85.
- Fogel SM, Smith CT (2011) The function of the sleep spindle: a physiological index of intelligence and a mechanism for sleep-dependent memory consolidation. *Neuroscience and biobehavioral reviews* 35:1154-1165.
- Franz O, Liss B, Neu A, Roeper J (2000) Single-cell mRNA expression of HCN1 correlates with a fast gating phenotype of hyperpolarization-activated cyclic nucleotide-gated ion channels (Ih) in central neurons. *The European journal of neuroscience* 12:2685-2693.
- Halliwel JV, Adams PR (1982) Voltage-clamp analysis of muscarinic excitation in hippocampal neurons. *Brain research* 250:71-92.
- Harnett MT, Magee JC, Williams SR (2015) Distribution and Function of HCN Channels in the Apical Dendritic Tuft of Neocortical Pyramidal Neurons. *The Journal of neuroscience : the official journal of the Society for Neuroscience* 35:1024-1037.
- He C, Chen F, Li B, Hu Z (2014) Neurophysiology of HCN channels: from cellular functions to multiple regulations. *Progress in neurobiology* 112:1-23.
- Huang H, Trussell LO (2014) Presynaptic HCN channels regulate vesicular glutamate transport. *Neuron* 84:340-346.
- Huang Z, Walker MC, Shah MM (2009) Loss of dendritic HCN1 subunits enhances cortical excitability and epileptogenesis. *The Journal of neuroscience : the official journal of the Society for Neuroscience* 29:10979-10988.
- Johnson JP, Jr., Zagotta WN (2005) The carboxyl-terminal region of cyclic nucleotide-modulated channels is a gating ring, not a permeation path. *Proceedings of the National Academy of Sciences of the United States of America* 102:2742-2747.
- Kanyshkova T, Meuth PB, P., Liu Z, Ehling P, Caputi L, Doengi M, Chetkovich DM, Pape HC, Budde T (2012) Differential regulation of HCN channel isoform expression in thalamic neurons of epileptic and non-epileptic rat strains. *Neurobiology of disease* 45:450-461.
- Kase D, Inoue T, Imoto K (2012) Roles of the subthalamic nucleus and subthalamic HCN channels in absence seizures. *Journal of neurophysiology* 107:393-406.

- Kesters D, Brams M, Nys M, Wijckmans E, Spurny R, Voets T, Tytgat J, Kusch J, Ulens C (2015) Structure of the SthK Carboxy-Terminal Region Reveals a Gating Mechanism for Cyclic Nucleotide-Modulated Ion Channels. *PloS one* 10:e0116369.
- Khazipov R, Sirota A, Leinekugel X, Holmes GL, Ben-Ari Y, Buzsaki G (2004) Early motor activity drives spindle bursts in the developing somatosensory cortex. *Nature* 432:758-761.
- Kole MH, Hallermann S, Stuart GJ (2006) Single Ih channels in pyramidal neuron dendrites: properties, distribution, and impact on action potential output. *The Journal of neuroscience : the official journal of the Society for Neuroscience* 26:1677-1687.
- Kopp-Scheinflug C, Pigott BM, Forsythe ID (2015) Nitric oxide selectively suppresses I currents mediated by HCN1 containing channels. *The Journal of physiology*.
- Kusile M, Wanaverbecq N, Brewster AL, Frere SG, Pinault D, Baram TZ, Luthi A (2006) Functional stabilization of weakened thalamic pacemaker channel regulation in rat absence epilepsy. *The Journal of physiology* 575:83-100.
- Levy R, Ashby P, Hutchison WD, Lang AE, Lozano AM, Dostrovsky JO (2002) Dependence of subthalamic nucleus oscillations on movement and dopamine in Parkinson's disease. *Brain : a journal of neurology* 125:1196-1209.
- Li M, Tonggu L, Tang L, Wang L (2015) Effects of N-glycosylation on hyperpolarization-activated cyclic nucleotide-gated (HCN) channels. *The Biochemical journal* 466:77-84.
- Lima MG, Maximino C, Matos Oliveira KR, Brasil A, Crespo-Lopez ME, Batista Ede J, Rocha FA, Picanco-Diniz DL, Herculano AM (2014) Nitric oxide as a regulatory molecule in the processing of the visual stimulus. *Nitric oxide : biology and chemistry / official journal of the Nitric Oxide Society* 36:44-50.
- Lolicato M, Nardini M, Gazzarrini S, Moller S, Bertinetti D, Herberg FW, Bolognesi M, Martin H, Fasolini M, Bertrand JA, Arrigoni C, Thiel G, Moroni A (2011) Tetramerization dynamics of C-terminal domain underlies isoform-specific cAMP gating in hyperpolarization-activated cyclic nucleotide-gated channels. *The Journal of biological chemistry* 286:44811-44820.
- Lorincz A, Notomi T, Tamas G, Shigemoto R, Nusser Z (2002) Polarized and compartment-dependent distribution of HCN1 in pyramidal cell dendrites. *Nature neuroscience* 5:1185-1193.
- Ludwig A, Budde T, Stieber J, Moosmang S, Wahl C, Holthoff K, Langebartels A, Wotjak C, Munsch T, Zong X, Feil S, Feil R, Lancel M, Chien KR, Konnerth A, Pape HC, Biel M, Hofmann F (2003) Absence epilepsy and sinus dysrhythmia in mice lacking the pacemaker channel HCN2. *The EMBO journal* 22:216-224.
- Ludwig A, Zong X, Jeglitsch M, Hofmann F, Biel M (1998) A family of hyperpolarization-activated mammalian cation channels. *Nature* 393:587-591.
- Macri V, Angoli D, Accili EA (2012) Architecture of the HCN selectivity filter and control of cation permeation. *Scientific reports* 2:894.
- Mangoni ME, Nargeot J (2008) Genesis and regulation of the heart automaticity. *Physiological reviews* 88:919-982.
- McCormick DA, Bal T (1997) Sleep and arousal: thalamocortical mechanisms. *Annual review of neuroscience* 20:185-215.
- McCormick DA, Pape HC (1990) Properties of a hyperpolarization-activated cation current and its role in rhythmic oscillation in thalamic relay neurones. *The Journal of physiology* 431:291-318.
- Michels G, Er F, Khan I, Sudkamp M, Herzig S, Hoppe UC (2005) Single-channel properties support a potential contribution of hyperpolarization-activated cyclic nucleotide-gated channels and If to cardiac arrhythmias. *Circulation* 111:399-404.

- Moosmang S, Biel M, Hofmann F, Ludwig A (1999) Differential distribution of four hyperpolarization-activated cation channels in mouse brain. *Biological chemistry* 380:975-980.
- Much B, Wahl-Schott C, Zong X, Schneider A, Baumann L, Moosmang S, Ludwig A, Biel M (2003) Role of subunit heteromerization and N-linked glycosylation in the formation of functional hyperpolarization-activated cyclic nucleotide-gated channels. *The Journal of biological chemistry* 278:43781-43786.
- Neuhoff H, Neu A, Liss B, Roeper J (2002) I(h) channels contribute to the different functional properties of identified dopaminergic subpopulations in the midbrain. *The Journal of neuroscience : the official journal of the Society for Neuroscience* 22:1290-1302.
- Nolan MF, Dudman JT, Dodson PD, Santoro B (2007) HCN1 channels control resting and active integrative properties of stellate cells from layer II of the entorhinal cortex. *The Journal of neuroscience : the official journal of the Society for Neuroscience* 27:12440-12451.
- Nolan MF, Malleret G, Dudman JT, Buhl DL, Santoro B, Gibbs E, Vronskaya S, Buzsaki G, Siegelbaum SA, Kandel ER, Morozov A (2004) A behavioral role for dendritic integration: HCN1 channels constrain spatial memory and plasticity at inputs to distal dendrites of CA1 pyramidal neurons. *Cell* 119:719-732.
- Nolan MF, Malleret G, Lee KH, Gibbs E, Dudman JT, Santoro B, Yin D, Thompson RF, Siegelbaum SA, Kandel ER, Morozov A (2003) The hyperpolarization-activated HCN1 channel is important for motor learning and neuronal integration by cerebellar Purkinje cells. *Cell* 115:551-564.
- Notomi T, Shigemoto R (2004) Immunohistochemical localization of Ih channel subunits, HCN1-4, in the rat brain. *The Journal of comparative neurology* 471:241-276.
- Pape HC, Mager R (1992) Nitric oxide controls oscillatory activity in thalamocortical neurons. *Neuron* 9:441-448.
- Pavlov I, Scimemi A, Savtchenko L, Kullmann DM, Walker MC (2011) I(h)-mediated depolarization enhances the temporal precision of neuronal integration. *Nature communications* 2:199.
- Paxinos G, Franklin KBJ (2008) *The Mouse Brain in Stereotaxic Coordinates*: Academic Press.
- Polack PO, Guillemain I, Hu E, Deransart C, Depaulis A, Charpier S (2007) Deep layer somatosensory cortical neurons initiate spike-and-wave discharges in a genetic model of absence seizures. *The Journal of neuroscience : the official journal of the Society for Neuroscience* 27:6590-6599.
- Polack PO, Mahon S, Chavez M, Charpier S (2009) Inactivation of the somatosensory cortex prevents paroxysmal oscillations in cortical and related thalamic neurons in a genetic model of absence epilepsy. *Cerebral cortex* 19:2078-2091.
- Poolos NP (2010) Genetic loss of HCN1 channels is exciting, but is it epileptic? *Epilepsy currents / American Epilepsy Society* 10:49-51.
- Prusky GT, West PW, Douglas RM (2000) Behavioral assessment of visual acuity in mice and rats. *Vision research* 40:2201-2209.
- Puljung MC, DeBerg HA, Zagotta WN, Stoll S (2014) Double electron-electron resonance reveals cAMP-induced conformational change in HCN channels. *Proceedings of the National Academy of Sciences of the United States of America* 111:9816-9821.
- Ryu S, Yellen G (2012) Charge movement in gating-locked HCN channels reveals weak coupling of voltage sensors and gate. *The Journal of general physiology* 140:469-479.
- Santoro B, Chen S, Luthi A, Pavlidis P, Shumyatsky GP, Tibbs GR, Siegelbaum SA (2000) Molecular and functional heterogeneity of hyperpolarization-activated pacemaker channels in the

- mouse CNS. *The Journal of neuroscience : the official journal of the Society for Neuroscience* 20:5264-5275.
- Santoro B, Grant SG, Bartsch D, Kandel ER (1997) Interactive cloning with the SH3 domain of N-src identifies a new brain specific ion channel protein, with homology to eag and cyclic nucleotide-gated channels. *Proceedings of the National Academy of Sciences of the United States of America* 94:14815-14820.
- Shah MM, Hammond RS, Hoffman DA (2010) Dendritic ion channel trafficking and plasticity. *Trends in neurosciences* 33:307-316.
- Strauss U, Kole MH, Brauer AU, Pahnke J, Bajorat R, Rolfs A, Nitsch R, Deisz RA (2004) An impaired neocortical Ih is associated with enhanced excitability and absence epilepsy. *The European journal of neuroscience* 19:3048-3058.
- Thon S, Schmauder R, Benndorf K (2013) Elementary functional properties of single HCN2 channels. *Biophysical journal* 105:1581-1589.
- Trevino M, Oviedo T, Jendritza P, Li SB, Kohr G, De Marco RJ (2013) Controlled variations in stimulus similarity during learning determine visual discrimination capacity in freely moving mice. *Scientific reports* 3:1048.
- van Luijteleaer G, Sitnikova E, Littjohann A (2011) On the origin and suddenness of absences in genetic absence models. *Clinical EEG and neuroscience* 42:83-97.
- Wahl-Schott C, Biel M (2009) HCN channels: structure, cellular regulation and physiological function. *Cellular and molecular life sciences : CMLS* 66:470-494.
- Wilkars W, Wollberg J, Mohr E, Han M, Chetkovich DM, Bähring R, Bender RA (2014) Nedd4-2 regulates surface expression and may affect N-glycosylation of hyperpolarization-activated cyclic nucleotide-gated (HCN)-1 channels. *FASEB journal : official publication of the Federation of American Societies for Experimental Biology* 28:2177-2190.
- Williams SR, Stuart GJ (2003) Voltage- and site-dependent control of the somatic impact of dendritic IPSPs. *The Journal of neuroscience : the official journal of the Society for Neuroscience* 23:7358-7367.
- Xue WN, Wang Y, He SM, Wang XL, Zhu JL, Gao GD (2012) SK- and h-current contribute to the generation of theta-like resonance of rat substantia nigra pars compacta dopaminergic neurons at hyperpolarized membrane potentials. *Brain structure & function* 217:379-394.
- Yang S, Cox CL (2007) Modulation of inhibitory activity by nitric oxide in the thalamus. *Journal of neurophysiology* 97:3386-3395.
- Yang S, Cox CL (2008) Excitatory and anti-oscillatory actions of nitric oxide in thalamus. *The Journal of physiology* 586:3617-3628.
- Yasoshima Y, Kai N, Yoshida S, Shiosaka S, Koyama Y, Kayama Y, Kobayashi K (2005) Subthalamic neurons coordinate basal ganglia function through differential neural pathways. *The Journal of neuroscience : the official journal of the Society for Neuroscience* 25:7743-7753.
- Ying SW, Kanda VA, Hu Z, Purtell K, King EC, Abbott GW, Goldstein PA (2012) Targeted deletion of Kcne2 impairs HCN channel function in mouse thalamocortical circuits. *PloS one* 7:e42756.
- Zong X, Krause S, Chen CC, Kruger J, Gruner C, Cao-Ehlker X, Fenske S, Wahl-Schott C, Biel M (2012) Regulation of hyperpolarization-activated cyclic nucleotide-gated (HCN) channel activity by cCMP. *The Journal of biological chemistry* 287:26506-26512.

[1]<http://neurolove.tumblr.com/post/2745681497/lets-breakdown-the-basal-ganglia-pathways-there#notes>

7. Appendix

7.1 Abbreviations

5-HT	serotonin
μg	microgram
μl	microliter
μm	micrometer
mm	minimeter
mV	minivolt
ALAS	<i>delta</i> -aminolevulinate synthase
Ach	<i>acetylcholin</i>
ap	<i>apathetic</i>
bp	base pair
BSA	bovine serum albumin
Ca ²⁺	calcium
CaCl ₂	calcium chloride
cAMP	cyclic adenosine monophosphate
cDNA	complementary DNA
cGMP	cyclic guanosine monophosphate
cm ²	square centimeter
cpm	counts per minute
CRB	cerebellum
CS ⁺	conditioned stimulus
CS ⁻	non-reinforced stimulus
C _t	threshold cycle
CT	corticothalamic
CTX	cortex
DD	diastolic depolarisation
ddH ₂ O	double deionized water
DEPC	diethyl pyrocarbonate
DNA	deoxyribonucleic acid

DNase	deoxyribonuclease
dNTP	2'-desoxynucleoside-5'-triphosphate (dATP, dCTP, dGTP, dUTP or dTTP)
DTT	dithiothreitol
e.g.	exempli gratia
EC	entorhinal cortex
EDTA	ethylenediaminetetraacetic acid
EEG	electroencephalography
EMG	electromyography
EPSP	excitatory postsynaptic potential
ERG	electroretinography
FP	forward primer
g	gram
GAPDH	glyceraldehyde 3-phosphate dehydrogenase
GAERS	Generalized Absence Epilepsy Rat from Strasbourg
GFP	green fluorescent protein
h	hour
HA	histamine
HCl	hydrochloric acid
HCN channel	hyperpolarization-activated cyclic nucleotide-gated channel
HEK cells	human embryonic kidney cells
HP	hippocampus
HRP	horseradish peroxidase
Hz	hertz
i.e.	id est
IHC	immunohistochemistry
IPS	<i>impulses per second</i>
Kb	kilo base pairs
kDa	kilo Dalton
KO	knockout
l	liter
I_h	h-current
I_T	low-threshold calcium current

IPSP	inhibitory postsynaptic potential
Lox	locus of X-ing over
MCS	multiple cloning site
M	molar
m	meter
MBq	megabecquerel
mCi	millicurie
mg	milligram
min	minute
mJ	milijoule
MiRP-1	MinK-related protein 1
ml	milliliter
mm	millimeter
mM	milimolar
MOPS	3-[N-Morpholino]propanesulfonic acid
mRNA	messenger RNA
NA	noradrenaline
$\text{Na}_2\text{HPO}_4 \cdot 2\text{H}_2\text{O}$	disodium hydrogen phosphate dihydrate
NaCl	sodium chloride
NaHCO_3	sodium bicarbonate
NaOH	sodium hydroxide
NGS	normal goat serum
nm	nanometer
NREM	non-rapid eye movement
NT	neurotransmitter
OB	olfactory bulb
OCT	optical coherence tomography
PAGE	polyacrylamide gel electrophoresis
p38 MAPK	p38 mitogen activated protein kinase
PBS	<i>phosphate</i> buffered saline
PCR	polymerase chain reaction
PFA	paraformaldehyde

PI	proteinase inhibitor
PM	post meridiem
pmol	picomol
PVDF	polyvinylidene difluoride
PVP	polyvinylpyrrolidone
qPCR	quantitative real-time PCR
REM	rapid eye movement
RNA	ribonucleic acid
Rnase	ribonuclease
RP	reverse primer
rpm	rotations per minute
RT	reverse transcription
RTN	reticular thalamic nuclei
RT-PCR	reverse transcriptase PCR
sec	second
SDS	sodium dodecylsulfate
SEM	standard error of the mean
SSC	saline-sodium citrate
ssRNA	single-stranded RNA
STN	subthalamic nuclei
SW	HCN2-1 switch mice
SWD	spike-and-wave discharge
Taq	<i>Thermus aquaticus</i>
TC	thalamocortical
TEA	triethanolamine
TEMED	N,N,N',N'-Tetramethylethylenediamine
TH	tyrosine hydroxylase
TH	thalamus
Tris	<i>tris</i> (hydroxymethyl)aminomethane
TSA	Tyramide Signal Amplification
Tx	Triton® X-100
U	unit

VB	ventral basal complex
UV	ultra violet
V _{0.5}	half maximal activation voltage
WAG/Rij	Wistar Albino Glaxo rats bred in Rijswijk
WB	western blot analysis
WT	wild-type
x g	gravitational force

7.2 Primers

7.2.1 HCN2-1 switch genotyping

Primer	Sequence (5'-3')
Geno_FP1	CCGAGAGGGTCCTGGGGAG
Geno_FP2	GGCGCGCCGCCGAGCGCAGCGTCTCATTAC
Geno_RP	GCACTGGAGAAGGGACAAGCAG

7.2.2 HCN1 genotyping

Primer	Sequence (5'-3')
IMR3410 F	CACCTGCTACGCAATGTTTG
IMR3411 R	ATTGGGCACTACACGCTAGG
IMR3412 F	AGAGAAATCATTCCCCGTGA

7.2.3 Primers for northern blot

Primer	Sequence (5'-3')
NB_mHCN1_E4_f	AAACAATATTCCTACGCACTC
NB_mHCN1_E4_r	ATACTGCCTCCTTGAAGAGT
NB_mHCN2E1E3_f	ATCATCCACCCCTACAGCG
NB_mHCN2E1E3_r	CATGTTGTTGATGGACACCC
mGAPDH_f	GGCAAATTCAACGGCACAGTC
mGAPDH_r	GTTTCTCCAGGCGGCACGTCA

7.2.4 Primers for *in situ* hybridization

Primer	Sequence (5'-3')
ISH_1E4_KpnI_f	AAAGGTACCAAACAATATTCCTACGCACTC
ISH_1E4_SacI_r	TAAGAGCTCATACTGCCTCCTGAAGAGT
ISH_2E1E3_KpnI_f	AATGGTACCATCATCCACCCCTACAGCG
ISH_2E1E3_SacI_r	TAAGAGCTCCATGTTGTTGATGGACACCC

7.2.5 Primers for qPCR

Primer	Sequence (5'-3')
HCN1_qPCR_E3_f	CTGCTGCAGGACTTCCCACCA
HCN1_qPCR_E4_r	ATGCTGACAGGGGCTTGGGC
HCN2_E1_qPCR_f	CAGGAACGCGTGAAGTCGGCG
HCN2_E2_qPCR_r	TCCAGGGCGCGGTGGTCTCG
HCN3_E7_qPCR_f	TGGCCATGGACCGGCTTCGG
HCN3_E8_qPCR_r	GAGCCAGGCCCGAACACCAC
HCN4_E7_qPCR_f	AGGGCCTTCGAGACGGTTGCGC
HCN4_E8_qPCR_r	GGCCATCTCACGGTCATGCCG

7.3 Primary antibodies

Antigen	Host	Company	Application	Dilution	TSA
HCN1	ms monoclonal	Abcam	WB	1:1000	-
HCN2	rb monoclonal	Alomone	WB/IHC	1:2000/1:300	-/yes
FLAG	ms monoclonal	Sigma, M2	WB	1:2000	-
ATPase	ms monoclonal	DSHB, α 6F	WB	1:1000	-
TH	rb monoclonal	Chemicon	WB/IHC	1:1000/1:300	-
HCN1	rb monoclonal	Alomone	IHC	1:100	yes

7.4 Secondary antibodies

Antigen	Host	Company	Application	Dilution
α -rb-HRP	donkey	Jackson laboratories	IHC	1:1000
α -ms-HRP	sheep	GE healthy	WB	1:1000
α -rb-HRP	donkey	Jackson laboratories	WB	1:2000
Alexa488 α -rb	F(ab') ₂	cell signaling	IHC	1:800
Dylight549 α -ms	donkey	Jackson laboratories	IHC	1:300

7.5 Alignment of the primary sequences of mHCN1 and mHCN2

mHCN1			DSSRRQ	YQEKYKQVEQ	YMSFHKLPA	415
mHCN2			DSSRRQ	YQEKYKQVEQ	YMSFHKLPA	468
mHCN1	MRQKIHDYEE	HRYQGKIFDE	ENILSELNDP	LREEIVNFNC	RKLVATMPLF	465
mHCN2	FRQKIHDYEE	HRYQGKMFDE	DSILGELNGP	LREEIVNFNC	RKLVASMPFL	518
mHCN1	ANADPNFVTA	MLSKLRFEVF	QPGDYIIREG	AVGKKMYFIQ	HGVAGVITKS	515
mHCN2	ANADPNFVTA	MLTKLKFVVF	QPGDYIIREG	TIGKKMYFIQ	HGVVSVLTKG	568
mHCN1	SKEMKLTGDS	YFGEICLLTK	GRRTASVRAD	TYCRLYSLSV	DNFNEVLEEY	565
mHCN2	NKEMKLSDGS	YFGEICLLTR	GRRTASVRAD	TYCRLYSLSV	DNFNEVLEEY	618
mHCN1	PMMRRAFETV	AIDRLDRIGK	KNSILLQKFQ	KDLNTGVFNN	QENEILKQIV	615
mHCN2	PMMRRAFETV	AIDRLDRIGK	KNSILLHKVQ	HDLSSGVFNN	QENAIIQEIV	668
mHCN1	KHDREMVQAI	PPINYPQMTA	LNCTSSTTTP	TSRMRTQSPP	VYTATSLSHS	665
mHCN2	KYDREMVQ--	-----	-----QAEL	QORVGLFPPP	PPPQVTSIAA	700
mHCN1	NLHSPSPSTQ	TPQPSAILS-	-----	-----	---PCSYTTA	691
mHCN2	TLQQAVAMSF	CPQ-----	-----	-----	-----	713
mHCN1	VCSPPIQSPL	ATRTRFHYASP	TASQLSLMQQ	PQQ--QLPQS	QVQQTQ--TQ	737
mHCN2	-VARPLVGPL	ALG-----	--SPRLVRRR	PPG--PLPPA	ASPGPP--AA	749
mHCN1	TQQQQQQQQQ	QQQQQQQQQQ	QQQQQQQQQQ	QQQQQQ--QQ	PQTPGSSTPK	785
mHCN2	SPPAAPSSPR	-----	-----	-----A	PRTSPYGVPG	770
mHCN1	NEVHKSTQAL	HNTNLTKEVR	PLSASQPS-L	PHEVSTLI--	SRPHPTVGES	832
mHCN2	SPATRVGPAL	PARRLSRASR	PLSASQPS-L	PHGVPAPS--	PAASARPASS	817
mHCN1	LASIPQPVA	VHSTGLQ---	AGSR-STVPQ	RVTLFRQMSS	GAIPPNRGVP	878
mHCN2	STPRLGPAPT	ARTAAPS---	PDRRDSASPG	AASGLDPLDS	ARSRLSSNL-	863
mHCN1	PAPPPPAAVQ	RESPSVLNTD	PDAEKPRFAS	NL		910
mHCN2	-----	-----	-----	--		

7.6 Nucleotide sequence of the HCN2-1 switch allele

	5' UTR of HCN2			***	FLAG-tag	
1	CCGCTCCGCT	CCGCACTGCC	CGGCGCCGCC	TCGCCATGGA	CTACAAAGAC	CATGACGGTG
						mHCN1
61	ATTATAAAGA	TCATGATATC	GATTACAAGG	ATGACGATGA	CAAGGAAGGC	GGCGGCAAAC
121	CCAACTCCGC	GTCCAACAGC	CGCGACGATG	GCAACAGCGT	CTTCCCCTCC	AAGGCGCCCG
181	CGACGGGGCC	GGTGGCGGCC	GACAAGCGCC	TGGGGACCCC	GCCGGGGGGC	GGCGCGGCCG
241	GGAAGGAACA	TGGCAACTCC	GTGTGCTTCA	AGGTGGACGG	CGGCGGAGGA	GAGGAGCCGG
301	CGGGCAGCTT	CGAGGATGCC	GAGGGGCCCC	GGCGGCAGTA	TGGTTTCATG	CAGAGGCAGT
361	TCACCTCCAT	GCTGCAGCCT	GGGGTCAACA	AATTCTCCCT	CCGCATGTTT	GGGAGCCAGA
421	AGGCGGTGGA	GAAGGAGCAG	GAAAGGGTTA	AAACTGCAGG	CTTCTGGATT	ATCCATCCGT
481	ACAGTGACTT	CAGGTTTTAT	TGGGATTTAA	TCATGCTTAT	AATGATGGTT	GGAAATTTGG
541	TCATCATAAC	AGTTGGAATC	ACGTTCTTCA	CAGAGCAGAC	GACAACACCG	TGGATTATTT
601	TCAACGTGGC	ATCCGATACT	GTTTTCTGT	TGGACTTAAT	CATGAATTTT	AGGACTGGGA
661	CTGTCAATGA	AGACAGCTCG	GAAATCATCC	TGGACCCTAA	AGTGATCAAG	ATGAATTATT
721	TAAAAAGCTG	GTTTGTGGTG	GACTTCATCT	CATCGATCCC	GGTGGATTAT	ATCTTTCTCA
781	TTGTAGAGAA	AGGGATGGAC	TCAGAAGTTT	ACAAGACAGC	CAGAGCACTT	CGTATCGTGA
841	GGTTTACAAA	AATTCTCAGT	CTCTTGCGGT	TATTACGCCT	TTCAAGGTTA	ATCAGATACA
901	TACACCAGTG	GGAAGAGATA	TTCCACATGA	CCTATGACCT	CGCCAGTGCT	GTGGTGAGGA
961	TCTTCAACCT	CATTGGCATG	ATGCTGCTTC	TGTGCCACTG	GGATGGCTGT	CTTCAGTTCC
1021	TGGTTCCCCT	GCTGCAGGAC	TTCCCACCAG	ATTGCTGGGT	TTCTCTGAAT	GAAATGGTTA
1081	ATGATTCTCTG	GGGAAAACAA	TATTCCTACG	CACTCTTCAA	AGCTATGAGT	CACATGCTGT
1141	GCATTGGTTA	TGGCGCCCAA	GCCCCTGTCA	GCATGTCTGA	CCTCTGGATT	ACCATGCTGA
1201	GCATGATTGT	GGGCGCCACC	TGCTACGCAA	TGTTTGTGG	CCATGCCACA	GCTTTGATCC
1261	AGTCTTTGGA	CTCTTCAAGG	AGGCAGTATC	AAGAGAAGTA	TAAGCAAGTA	GAGCAATACA
1321	TGTCATTCCA	CAAGTTACCA	GCTGACATGC	GCCAGAAGAT	ACATGATTAC	TATGAGCACC
1381	GATACCAAGG	CAAGATCTTC	GATGAAGAAA	ATATTCTCAG	TGAGCTTAAT	GATCCTCTGA
1441	GAGAGGAAAT	AGTCAACTTC	AACTGCCGGA	AACTGGTGGC	TACTATGCCT	CTTTTTGCTA
1501	ACGCCGATCC	CAATTTCTGTG	ACGGCCATGC	TGAGCAAGCT	GAGATTTGAG	GTGTTCCAGC
1561	CCGGAGACTA	TATCATTCGA	GAAGGAGCTG	TGGGGAAGAA	AATGTATTTT	ATCCAGCACG
1621	GTGTTGCTGG	CGTTATCACC	AAGTCCAGTA	AAGAAATGAA	GCTGACAGAT	GGCTCTTACT
1681	TCGGAGAGAT	ATGCCTGCTG	ACCAAGGGCC	GGCGCACTGC	CAGTGTCCGA	GCTGATACCT
1741	ACTGTCGTCT	TACTCCCTT	TCGGTGGACA	ATTTCAATGA	GGTCTTGAG	GAATATCCAA
1801	TGATGAGAAG	AGCCTTTGAG	ACAGTTGCTA	TTGACCGACT	CGATCGGATA	GGCAAGAAAA
1861	ACTCTATTCT	CCTGCAGAAG	TTCCAGAAGG	ATCTAAACAC	TGGTGTTTTC	AACAACCAGG
1921	AGAACGAGAT	CCTGAAGCAG	ATCGTGAAGC	ATGACCGAGA	GATGGTACAA	GCTATCCCTC
1981	CAATCAACTA	TCCTCAAATG	ACAGCCCTCA	ACTGCACATC	TTCAACCACC	ACCCCAACCT

2041 CCCGCATGAG GACCCAATCT CCGCCAGTCT ACACCGCAAC CAGCCTGTCT CACAGCAATC
 2101 TGCACTCACC CAGTCCCAGC ACACAGACGC CCCAACCCCTC AGCCATCCTT TCACCCTGCT
 2161 CCTATACCAC AGCAGTCTGC AGTCCTCCTA TACAGAGCCC CCTGGCCACA CGAACTTTCC
 2221 ATTATGCCTC TCCCCTGCG TCCCAGTGT CACTCATGCA GCAGCCTCAG CAGCAACTAC
 2281 CGCAGTCCCA GGTACAGCAG ACTCAGACTC AGACTCAGCA GCAGCAGCAG CAACAGCAGC
 2341 AGCAGCAGCA GCAGCAACAG CAACAACAGC AGCAGCAGCA GCAGCAGCAG CAGCAGCAGC
 2401 AGCAGCAGCA GCAGCAGCAG CAGCAGCCAC AGACACCTGG TAGCTCCACA CCGAAAAATG
 2461 AAGTGCACAA GAGCACACAA GCCCTTCATA ACACCAACCT GACCAAAGAA GTCAGGCCCC
 2521 TTTCCGCCTC GCAGCCTTCT CTGCCCATG AGGTCTCCAC TTTGATCTCC AGACCTCATC
 2581 CCACTGTGGG CGAATCCCTG GCCTCTATCC CTCAACCCGT GGCAGCAGTC CACAGCACTG
 2641 GCCTTCAGGC AGGGAGCAGG AGCACAGTGC CACAACGTGT CACCTTGTTT CGACAGATGT
 2701 CCTCGGGAGC CATCCCCCCC AACCGAGGAG TGCCTCCAGC ACCCCCTCCA CCAGCAGCTG
 2761 TGCAGAGAGA GTCTCCCTCA GTCCTAAATA CAGACCCAGA TGCAGAAAAA CCCCCTTTTG

 *** 3' UTR of HCN2
 2821 CTTTCGAATTT ATGACCCTTG AGCGCCGCC CGCGGGCCGG GCGGGGCCGT CATCCACACC
 2881 AAAGCCATGC CTCGCGCCGC CCGCCCGTGC CCGTGCAGAA GCCATAGAGG GACGTAGGTA
 2941 GCTTAGGAGG CGGGCGGCC TGCGCCCGGC TGTCCCCCA TCGCCCTGCG CCCACCCCA
 3001 TCGCCCCTGC CCCAGCGGCG GCCGCACGGG AGAGGGAGGG GTGCGATCAC CTCGGTGCCT
 3061 CAGCCCCAAC CTGGGACAGG GACAGGGCGG CCCTGGCCGA GGACCTGGCT GTGCCCGCA
 3121 TGTGCGGTGG CCTCCGAGGA AGAATATGGA TCAAGTGCAA TACTCGGCC GCCGGCTTCC
 3181 CGCTGCCCCCT GGCAAGCTCA CGCAATAACC AGCCCGCCCC TGCCCACGCG TCCGTGGTGA
 3241 CCTCCCTCGG GCACCCAGGG GCGGGCTTCA CGGCCAAGCC GGCCTGGGG TGAGGCTGGG
 3301 TCCCCGCCGT CGCCATGAAT GTACTGACGA GCCGAGGCAG CAGTGGCCCC CACGCCCAT
 3361 TAACCCACAA CCCCATTCG CGCAATAAAC GACAGCATTG GCGGCGCGCC GCCGAGCGCA
 3421 GCGTCTCATT ACTTTGGTGG GTTTGCGCAC CGCCAGAAAG TGGCGGCTGG CATAGGTAGA
 3481 CACAACTTT CATTATTTA CATTATGCAC AGGTTTAGGG ACCGCATGGC GTGGGGGCGC

LoxP
 3541 GCCCTTAAGT CTAGATATCG ATGAATTCAT AACTTCGTAT AATGTATGCT ATACGAAGTT
 3601 ATGGATCTGT CGATCGACGG ATCGATCCGA ACAAACGACC CAACACCCGT GCGTTTTATT
 3661 CTGTCTTTTT ATTGCCGATC CCCTCAGAAG AACTCGTCAA GAAGGCGATA GAAGGCGATG
 3721 CGCTGCGAAT CGGGAGCGGC GATACCGTAA AGCACGAGGA AGCGGTCAGC CCATTGCCG
 3781 CCAAGCTCTT CAGCAATATC ACGGGTAGCC AACGCTATGT CCTGATAGCG GTCCGTCTTA

* start/stop codon

7.7 Acknowledgement

First of all, I would like to give my sincere gratitude to my supervisor, Prof. Martin Biel, for providing me the best opportunity to complete Ph.D. dissertation in his laboratory. He taught me how to think as a scientist and gave me so many invaluable chances to prove and improve myself. I would like to express my deepest thanks to Dr. Verena Hammelmann, who has being my supervisor since my Master study. Without her priceless patience, tremendous assistance and inspiring discussions, this dissertation would not have been done. Many thanks were given to Saskia Spahn and Christian Schön, who kindly performed the EEG and the OCT measurement, respectively. I would also like to thank all my colleagues. They are very nice and help me to improve the German language every day. I will never forget any minute with them wherever I am. Big thanks to my friends in Munich, I feel so lucky to have them around. The most special thanks I would like to express to my lovely family, their encouragement supports me to go further and makes me not feel alone.